POLITECNICO DI TORINO

Faculty of Engineering
Course of Mechatronic Engineering

Master Thesis

Airborne Wind Energy:

Development of a flying traction sensing system and integration of a wind monitoring system for extreme weather conditions

Relatori
Prof. Claudio Sansoe'
Prof. Paolo Maggiore

Referente Aziendale
Ing. Paolo Petrini

Candidato
Riccardo Cortese

Spring 2019

A Mamma e Papà. A Luna.

Sommario

Temperature torride, incendi, siccità e nubifragi. Tra Luglio 2018 e Novembre 2018 intere regioni del pianeta, dal Giappone alla Scandinavia, dalla California alla Giordania, hanno vissuto condizioni climatiche estreme. Senza un netto cambio di rotta, l'umanità rischia di perdere la lotta contro il riscaldamento globale. Via via che gli effetti del cambiamento climatico diventano più evidenti, le sfide che ci attendono si fanno più complicate. A tre anni dall'accordo di Parigi, in cui 195 paesi si sono impegnati a mantenere il riscaldamento *"ben al di sotto di due gradi"* rispetto al livello preindustriale, le emissioni di gas serra sono aumentate ancora. Nel 2017 la domanda di carbone è aumentata per la prima volta in quattro anni. In molti paesi i sussidi per le energie rinnovabili stanno diminuendo e gli investimenti sono bloccati. Il nucleare, meno dannoso in termini di produzione di CO_2, è costoso e impopolare. La difficoltà tecnica di eliminare il carbone dalle industrie in generale, non solo da quelle che producono energia, è quanto mai concreta. L'acciaio, il cemento, l'agricoltura e i trasporti sono responsabili di più della metà delle emissioni di carbonio del pianeta. Tecnicamente queste attività sono più difficili da ripulire rispetto ai processi con cui si produce l'energia, anche per via dell'entità degli interessi in gioco. Fermare il cambiamento climatico ha senz'altro dei costi a breve termine, ma alla fine la rinuncia ai combustibili fossili arricchirà l'economia. In questo scenario la politica gioca un ruolo chiave con l'industria e le università, che devono lavorare in sinergia sviluppando nuove tecnologie, promuovendo politiche di sviluppo sostenibili a tutto tondo, disincentivando visioni strategicamente miopi e a breve termine e favoreggiando il consolidamento di un mercato le cui dinamiche siano concordi e convergenti intorno la sostenibilità ambientale.

La seguente tesi riguarda lo sviluppo di un sistema di monitoraggio e rilevamento delle tensioni lungo le briglie di un aquilone al fine di poter migliorare l'efficienza di una tecnologia innovativa ed emergente per la generazione di energia elettrica sfruttando i venti ad alta quota. Il lavoro è stato svolto analizzando il contesto ed il problema, proponendo un sistema sensoristico in grado di effettuare le misure adeguate che fosse minimamente invasino e non intralciasse in alcun modo le operazioni di volo. I sensori sono stati quindi caratterizzati ed integrati nel prototipo di Kitenergy s.r.l. dal nome KE60 mark II. In aggiunta è stata integrata nello stesso prototipo una stazione meteo in grado di monitorare l'intensità del vento e la sua direzione a 10m dal suolo con il fine di acquisire data set utili e robusti che possano esser utilizzati all'interno di una catena di controllo che permetta di effettuare le operazioni di volo in maniera totalmente automatizzata.

Ai tempi di Loyd i sistemi AWE sembravano una visione più che una concreta alternativa. Oggi i continui progressi sui cavi e sulle aerostrutture, sui controlli automatici e sui sitemi di navigazione aprono un nuovo scenario ad un manipolo di sognatori che sperimenta queste tecnologie raggiungendo risultati concreti ogni anno avvicinandosi sempre più alla meta finale: energia pulita e rinnovabile per tutti.

Abstract

Sweltering temperatures, fires, droughts and rainstorms. Between July 2018 and November 2018 entire regions of the world, from Japan to Scandinavia, from California to Jordan, have experienced extreme weather conditions. Without a course change, humanity risks to lose the fight against global warming. As the effects of climate change becomes more evident, the challenges becomes more complicated. It's been three years from the Paris conference, in which 195 countries committed to keep global warming *"more than two degrees"* below the pre-industrial levels, but the greenhouse gas emissions have still increased. In 2017 the demand of carbon raised for the first time in four years. In many countries grants for renewable energies are decreasing and investments are blocked. Nuclear energy, less dangerous in terms of CO_2 production, is expensive and unpopular. The technical difficulty of banishing carbon from industries, not only from those who produce energy, is real. Steel, cement, agriculture and transportation are responsible for more than half of carbon emissions of the planet. Technically, these activities are more difficult to clean if compared to the processes that produce energy, also because of the interests that are involved. Stop climate change has without a doubt a price in the short-term, but in the end giving-up on fossil fuels will enrich the economy. In this scenario, politics play a key role along with industry and universities that must cooperate in synergy developing new technologies, promoting real sustainable policies for development, discouraging strategically short-sighted visions and encouraging the strengthening of a market whose dynamics should be concurrent and convergent in terms of environmental sustainability.

The current master thesis is about the deployment of a monitoring and detecting system along the bridles of a kite, improving the efficiency of a innovative and emerging technology for high altitude wind energy generation. The work has been done analyzing the context and the problem, proposing a minimally invasive sensing system able to correctly acquire data and not to hinder with the flight operations at all. The sensors have been characterized and integrated into the prototype developed by Kitenergy s.r.l. named KE-60 mkII. Furthermore, a weather station has been integrated in the same prototype, to detect and monitor wind intensity and direction at ground level. The scope of this weather station is to acquire useful data for the development of a control chain that will allow the flight operations to be totally autonomous.

If at Loyd's time the AWE technology seemed a vision, nowadays the continuous progresses in tether and wing materials, in automatic control and in navigation technologies are opening a total new scenario for a fists of entrepreneurs that are working on this new technology achieving outstanding milestones every year for final goal: clean and totally renewable energy for all.

Acknowledgements

Con la presente vorrei profondamente ringraziare tutte le persone che mi sono state vicino in questi anni e che mi hanno accompagnato in questo cammino, rendendolo leggero.
Loro sanno chi sono.

Vorrei inoltre ringraziare il team di Kitenergy per il lavoro svolto insieme.

Contents

List of Figures

List of Tables

Chapter 1

Introduction

This chapter will briefly an actual global energy perspective, focusing on the active role of renewable energies with a particular care to emerging technologies in the wind power field.

1.1 Past and present of world energy

In 2016, non-OECD countries's share of production reached 56.2% of world electricity generation, double the share they held in 1974, reflecting the higher average growth rate which has prevailed in the non-OECD regions since 2000. In 2016, still, generation from combustible fuels accounted for 676.3% of total world gross electricity production, while hydroelectric plants provided 16.6%, nuclear plants 10.4%; geothermal, solar, wind, tide and other sources 5.6%; and biofuels and waste made up the remaining 2.3%.

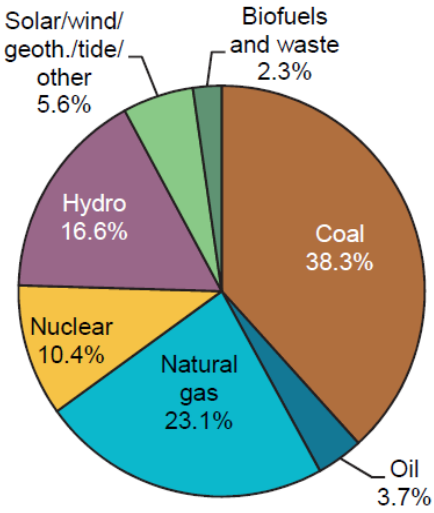

Figure 1.1: World gross electricity production, by source, 2016.

Between 2016 and 2017, though, a decrease in electricity production from fossil fuels has been registered, with declines observed in output from oil (-7.2%), natural gas (-1.6%), and coal (-1.1%). There were also declines in generation from nuclear (-0.7%) and hydroelectric plants (-0.7%), probably due to scheduled maintenance and variations in weather patterns, respectively. An interesting fact is that electric-

ity generation from renewable sources such as wind (+15.1%) and solar (+21.9%) registered robust growth.

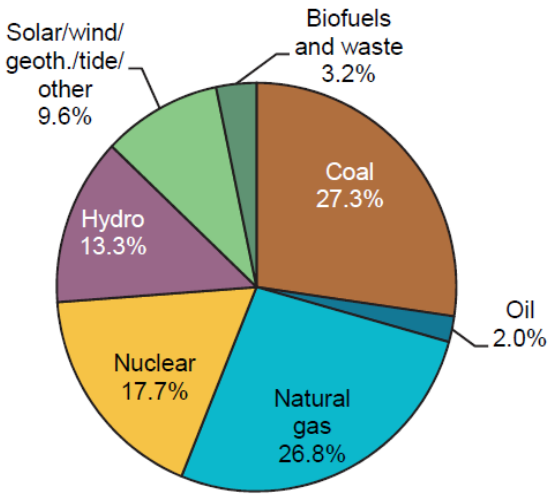

Figure 1.2: World gross electricity production, by source, 2017. IEA 2018.

In terms of production shares, 2017 was similar to 2016, with gas generation virtually matching coalfired generation across the OECD, at 26.8% and 27.3% respectively. Renewables and waste combined was also around this figure, at 26.1%, whilst nuclear made up just under a fifth of total generation (17.7%). In 2011, non-OECD electricity production surpassed OECD production for the first time, and its share of production has continued to increase since then.

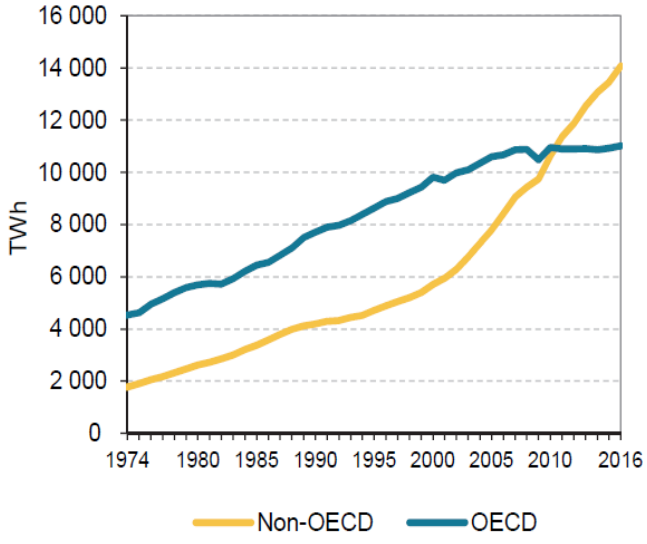

Figure 1.3: Total gross electricity production. IEA 2018.

Despite the desperate need for early emission reduction, the world is not moving towards the Paris goals but rather away from them, thus the CO_2 emissions are set to increase in 2018, again. However, it is true that there is a remarkable growth of electricity generation from renewable sources, especially distributed among the OECD countries, but this is clearly not enough to achieve the goals set in Paris in 2015: limiting the global temperature rise below 2 Celsius degrees. Even with

ongoing cost reduction, government policy remains crucial to attract investments in renewable energies, ensure appropriate market design and for reliable, cost-effective system integration. Even though the usage of renewable energies is set to rise for the coming years, a greater use of solar, wind, bioenergy and other renewables is needed in all sectors for emissions to peak immediately then decline.

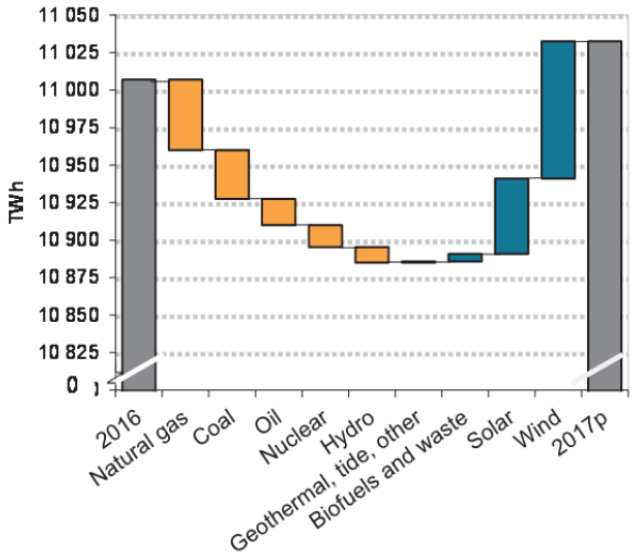

Figure 1.4: OECD gross electricity production variation, 2016-2017. IEA 2018.

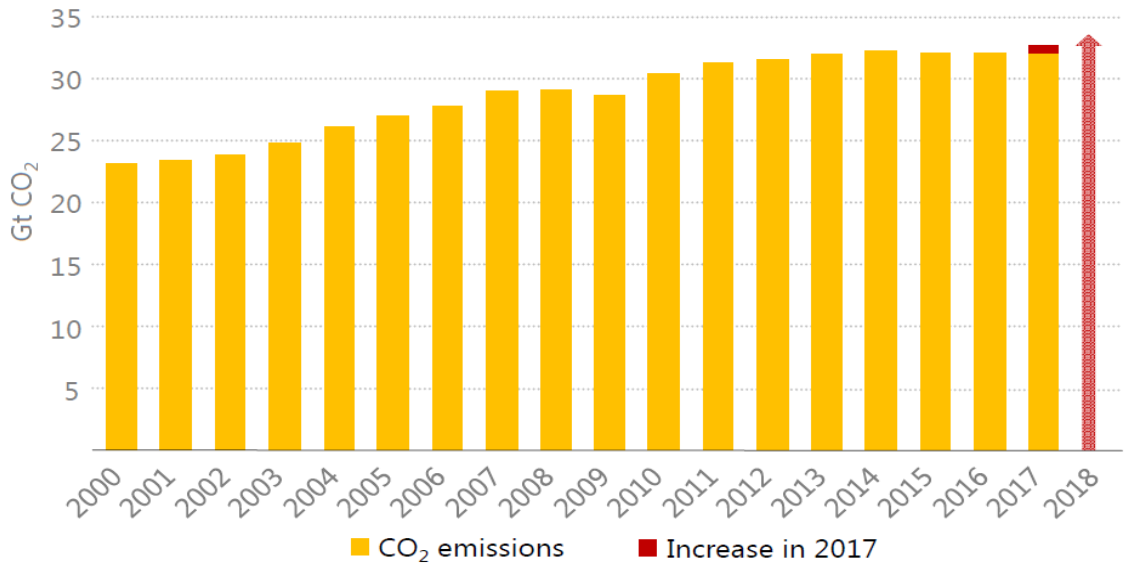

Figure 1.5: Global CO_2 emissions. IEA 2018.

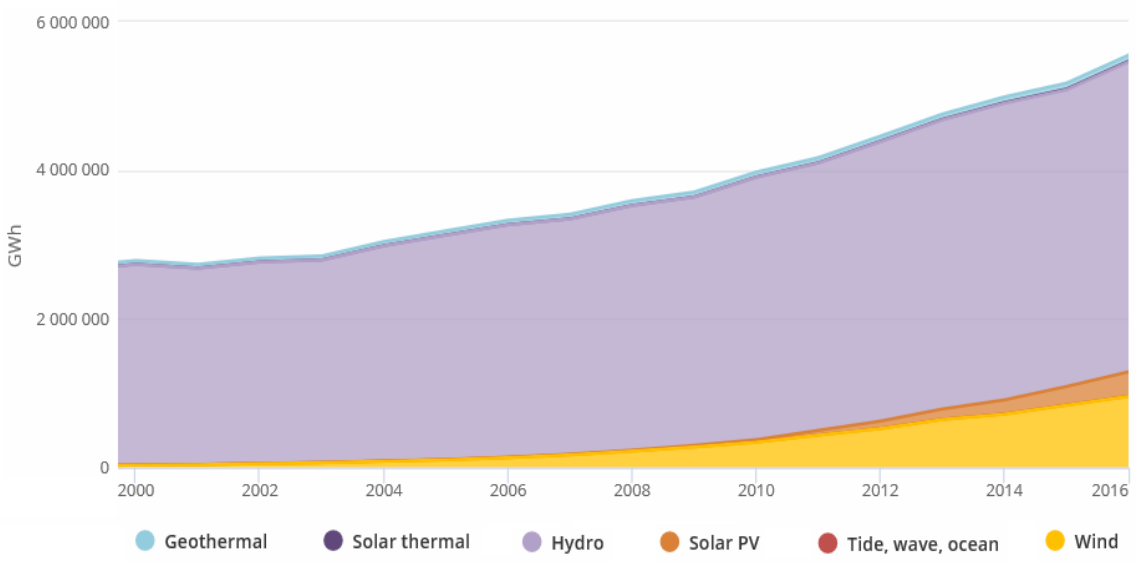

Figure 1.6: Electricity generation from renewable by source. IEA 2018.

1.2 Wind energy

The wind blows because of precise atmospheric phenomena that are out of the scope of this paper, but it is out of doubt that the recent climate changes are cause of various problems in the wind energy sector. Specifically, wind as a moving mass is characterized by a direction and a velocity that can be measured and compared to various scales and systems in order to have a practical sense of the weather condition. The recent shifts in temperature are affecting humidity, wind intensity and directions all over the world so that many places that were considered calm most of the year are experiencing strong gales, or in some cases even storms, that can be considered completely out of standards. However, wind energy is a prominent player within the renewable sources panorama in terms of technology efficiency and electricity generation. It is widely distributed, clean, affordable, abundant, requires a non-earthy surface and is not responsible for greenhouse gas emissions during operation. Moreover, wind energy is a very robust alternative to fossil fuels.

As said before, wind energy may be considered stable during a year, but has significant variations on shorter time windows. It is thus very important to know various type of data regarding local weather, such as wind speed and direction, wind variations with the quota, day-time, nigh-time and seasonal changes, amount of gusts in the short periods and the peaks intensity over at least twenty years. Regarding wind intensity the Beaufort's scale is widely adopted by the EU countries, ranging from 0 to 12 and providing a brief description of the effects.

Giving wind velocity and direction in knots is also a valid and widely accepted method to describe wind force. This data are usually given by some weather stations that are able to detect wind intensity and direction. Typically a bowl anemometer is used, combined with a wind vane. Usually a fully equipped weather station is able to collect data by monitoring various physical quantities such as solar radiation by means of a pyranometer, visibility, rain and snow. Flying a kite to exploit the kinetic energy of wind and, by transforming it into usable mechanical power and than to electric power, generating electricity is a matter of knowing local atmospheric conditions but, first of all, local wind characteristics.

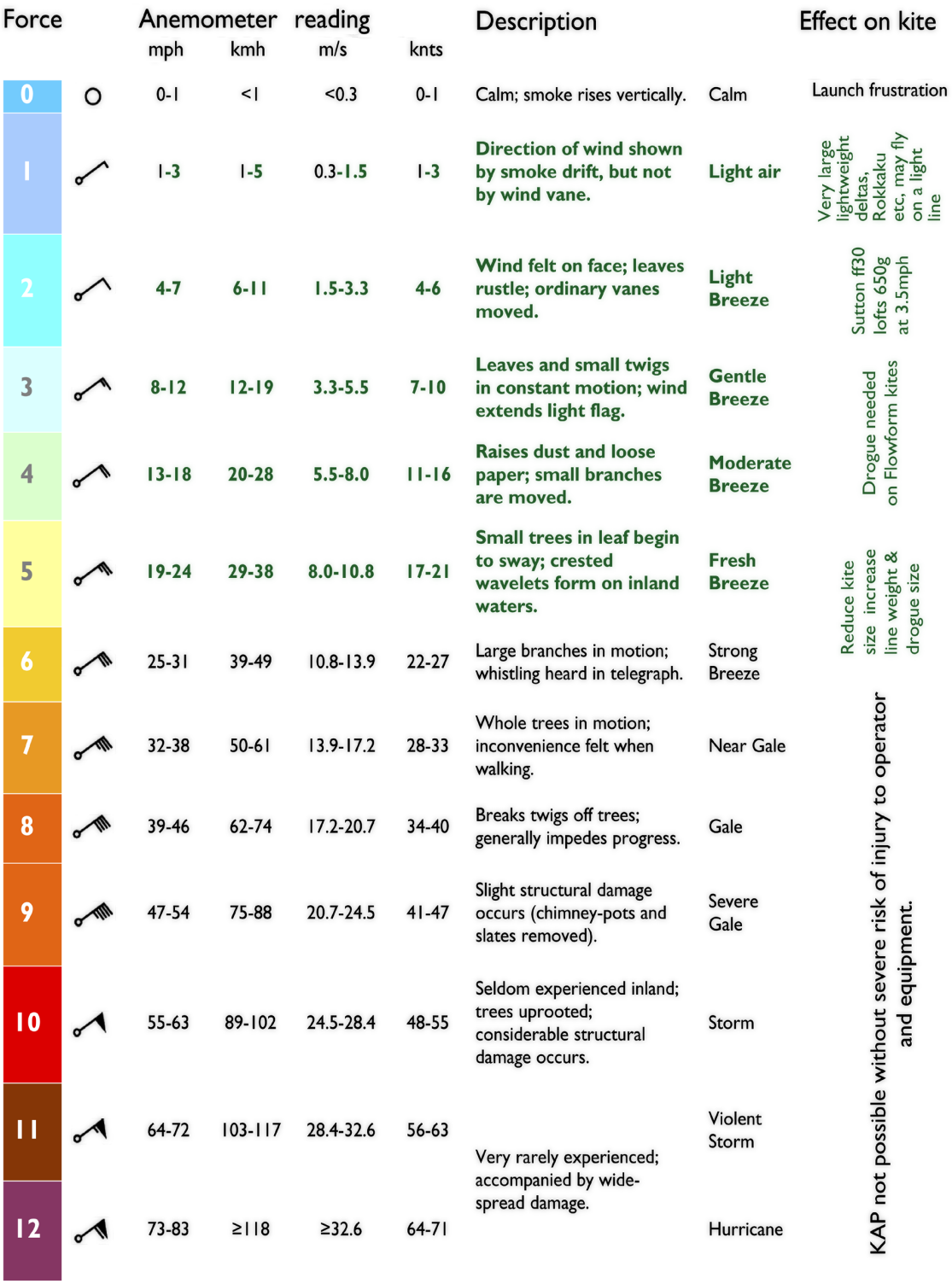

Figure 1.7: Beaufort's scale.

Benefits of wind energy

The popularity of wind energy arises from the simple fact that it is, by and large, cost effective, environmentally friendly and socially popular amongst a majority of the populace. A common method of assessing the cost-effectiveness of an energy source is through a parameter called Levelized Cost of Energy (LCOE), which is essentially a ratio between two parameters: the total lifetime costs and the total electricity produced over the lifetime. Siemens calculated in 2014 the LCOE of various electricity generation sources to be as follows:

As Table 1.1 shows, the LCOE of onshore wind is reasonably close to the LCOE of commonly used fossil fuels. However, the LCOE alone does not often provide the complete picture.

A more comprehensive measure, as provided by Siemens still in 2014 is the so-called Society's Cost of Energy (SCOE). The SCOE takes into consideration further factors such as number of jobs created by energy source, subsidies, transmission costs, variability costs, geopolitical risk impact, and environmental impact. The predicted SCOE in the year 2025 for various electricity generation sources is shown in Table 1.2.

Source of electricity generation	LCOE (AC/MWh)
Nuclear	79
Coal	63
Gas	60
Photovoltaics	145
Onshore wind	81
Offshore wind	140

Table 1.1: LCOE in 2013 for various electricity generation sources

Source of electricity generation	SCOE (AC/MWh)
Nuclear	107
Coal	110
Gas	89
Photovoltaics	78
Onshore wind	60
Offshore wind	61

Table 1.2: SCOE in 2025 for various electricity generation sources

As shown in Table 1.2, it is expected that onshore and offshore wind will be the two most viable sources of energy in the near future. In fact, this phenomenon is already manifesting — statistics indicate the benefits from wind energy to be significant. As an example of the social benefits of wind energy, the Global Wind Energy Council (GWEC) estimates that more than 600,000 people are employed by the wind industry — a number that is likely to rise to more than 2,000,000 by 2030. In terms of a positive environmental impact, wind energy helped to avoid more than 608 million tonnes of carbon dioxide emissions in 2014 alone. GWEC also estimate that wind farms generate between 17 and 39 times more power than they consume — compared to 16 times for nuclear and 11 times for coal plants.

1.3 Wind turbines

The kinetic energy of wind is converted into usable mechanical power by means of mechanical devices that are able to convert torque into electrical power. In particular, the appliance of this principle is stressed at is plateau in wind turbines. On the market, wind turbines have different shapes and heights and based on their position with respect to the wind, they may be divided into two main categories.

1. Horizontal axis wind generators, in which the rotor must be parallel with respect to wind orientation;

2. Vertical axis wind generators, in which the rotor is independent to wind orientation;

Modern wind generators belong to the first category, but still present a certain variety in design and scale that should be briefly discussed along with some highlights about the cost of design, installation, operating and, more over, decommissioning.

Generally speaking, the generational wind turbine system is composed as in Figure 1.8, where two different construction models are presented. Gearboxes typically have the advantage of requiring smaller initial investments, but because of the number of rotating parts, gear pairs and bearings, reliability is typically an issue. On the other hand, direct-drive machines require a bigger investment related to the development and construction of big permanent magnet generators but have typically lower operation and maintenance costs. To guarantee the effectiveness and competitiveness of the gearbox solution, significant improvements in the design phase are required to better understand the mechanisms leading to gearbox failures. This can only be achieved by developing more accurate, reliable and efficient numerical models, able to replicate not only the global load transfer paths across the driveline but also the local load transfer mechanisms. Besides the power transfer system, the numbers of blades are usually set to three, even thought five blades are more efficient in terms of power production. The main reason why the three blade rotor is much more widely spread, is because of the cost of production and installation. Not only the cost of the blades is remarkable if compared to the total tower, but in the case of five blades it will rise at the point of overcoming the benefits of building a wind turbine. An other factor that is important to mention, is the construction process. The blades, that can easily reach 100m of length, have to be transported on the site which is often located in not so accessible areas, for example mountains, hills or even offshore. Once on the field, the blades have to be installed on the rotor and integrated one after the other. This means mechanically stressing the structure with important loads that may be harmful to the generation system and to the structure itself. Lastly, there is the weight factor: having five blades against three increases the total weight of the structure and significantly increases the chances of failure of various systems. Thus three rotor blades are much more common nowadays even though the power outcome is slightly lower, mainly because of the cost that increases significantly with the volume of material used.

Roughly, the power output of a wind turbine is given by the following expression

$$P = \frac{1}{2} C_P \rho A v_w^3 \tag{1.1}$$

where ρ is the air density ($1.225 kg/m^3$), C_P is the power coefficient, A is the rotor swept area and v_w is the wind speed. It should be noticed that the wind speed is the

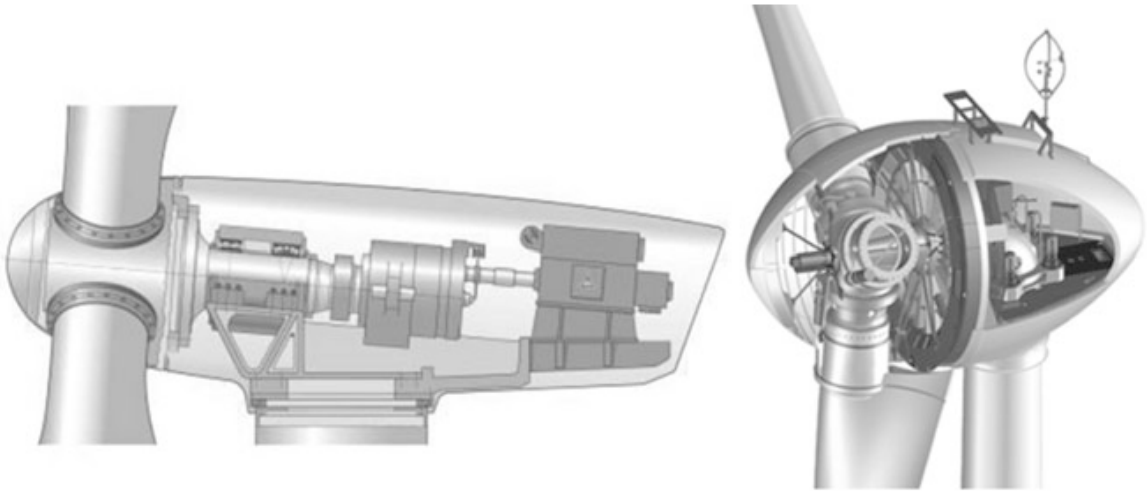

Figure 1.8: Typical turbine driveline configurations. Gearbox on the left, Direct-drive generator on the right.

most important factor in the equation due to its presence in the cubic form. This means that a very small increase in wind intensity produces a significant outcome in terms of electrical power production. The power coefficient describes the fraction of power that the turbine is able to extract from the wind and convert into mechanical work; it has ha maximum value though, also known as the Betz limit, that is 0.593: this means that the wind turbine is able to extract up to 59% of the energy contained in the airflow thought its actual working area.

There are some limits in wind intensity for the wind turbine to properly work. If the wind is below $3m/s$ the force acting on the blades is simply too low overcome the motor inertia and produce power. If wind speed overcomes the upper limit, usually around $25m/s$, the wind turbine sets itself at out of service to maintain its integrity by pitching the blades to stop power production and rotation. Furthermore, due to its intrinsic nature, wind doesn't blow constantly all over the year, thus wind generators cannot produce continuously rated power. The average power produced over the year, indicated as Capacity Factor (CF), is a fraction of its rated power. The CF is evaluated by considering the probable density and distribution of wind speed across the interested area and the power curve of the generator. To maximize the CF, wind turbines need to be reach important height because of the wind shear for which the wind speed grows along with the elevation. In the table below the properties of the 10 MW DTU wind turbine are reported, while in Figure 1.9 the power curve of the same commercial wind turbine is shown.

1.4 From wind turbines to high altitude wind generation

Airborne wind energy(AWE), regards the generation of usable power by airborne devices. All airborne wind energy systems with significant power output are mechanically connected to the ground in order to exploit the relative velocity between the air mass and the ground: most of the companies around the world that have achieved relevant milestones are using tethers. The most common strategy is to fly a kite in crosswind direction: the reason for this is because

10 MW DTU wind turbine	
Parameter	Value
Rating	10 MW
Rotor orientation, configuration	Upwind, three blades
Control	Variable speed, collective pitch
Drivetrain	Medium speed, multiple stage gearbox
Rotor, hub diameter	178.3 m, 5.6 m
Cut-in, rated, cut-out wind speed	4 m/s, 11.4 m/s, 25 m/s
Cut-in, rated rotor speed	6 RPM, 9.6 RPM
Rated tip speed	90 m/s
Overhang, shaft tilt, pre-cone	7.07 m, 5°, 2.5°
Pre-bend	3m
Rotor mass	229 tons (each blade around 41 tons)
Nacelle mass	446 tons
Tower mass	605 tons

Table 1.3: Properties of the 10 MW DTU wind turbine

$$F_L = \frac{1}{2}\rho A C_L v_a^2 \tag{1.2}$$

where ρ is the density of the air, A the airfoil area, C_L the lift coefficient which depends on the geometry of the kite or of the wings. Thus, if a kite is flown with v_a that is ten times faster than the wind speed v_w, the tension in the line increases by a factor of hundred in comparison to a kite that is kept at a static position in the sky. The high speed of the kite can be maintained by the ambient wind flow, and the tether tension can be made useful for harvesting a part of the enormous amount of power that the moving wing can potentially extract from the wind field. Comparing crosswind kite power systems with conventional wind turbines, it's possible to assume, from a certain perspective, that the idea of the AWE is to build the fastest moving part of a large wind turbine, which are the tips of the rotor blades, and to replace them with automatic controlled fast flying tethered wings. The cause of this has to be researched into the wind turbines nature itself: the outer 30% of the blades provide more than half of the total power. In facts, the power P that can be generated with tethered airfoil, as discussed by Loyd, is approximately given by:

$$P = \frac{2}{27}\rho A v_w^3 C_L \Big(\frac{C_L}{C_D}\Big)^2 \tag{1.3}$$

where A is the area of the wing, C_L the lift and C_D drag coefficients and v_w is the wind speed. It's important to note that the lift-to-drag ration is present in the formula quadratically and thus plays a relevant role in the AWE systems. This factor is known in aerospace as the *gliding number* that describes how a glider without propulsion is able to move horizontally compared to its vertical sink rate. As stated by Diehl in *Airborne Wind Energy*, if a modern wing with $C_L = 1$ and and intrinsic $C_D = 0.03$, with a $v_w = 13$ m/s would lead to a power of 217 kW per m^2 wing area. Unfortunately the drag caused by the tether is significant, thus a more realistic value is $C_D = 0.07$ which leads to a theoretical power output of $P =$ 40 kW per m^2 of wing area. This has not been achieved by any AWE companies yet.

It's important to remember that the impressive saving in material, that is the

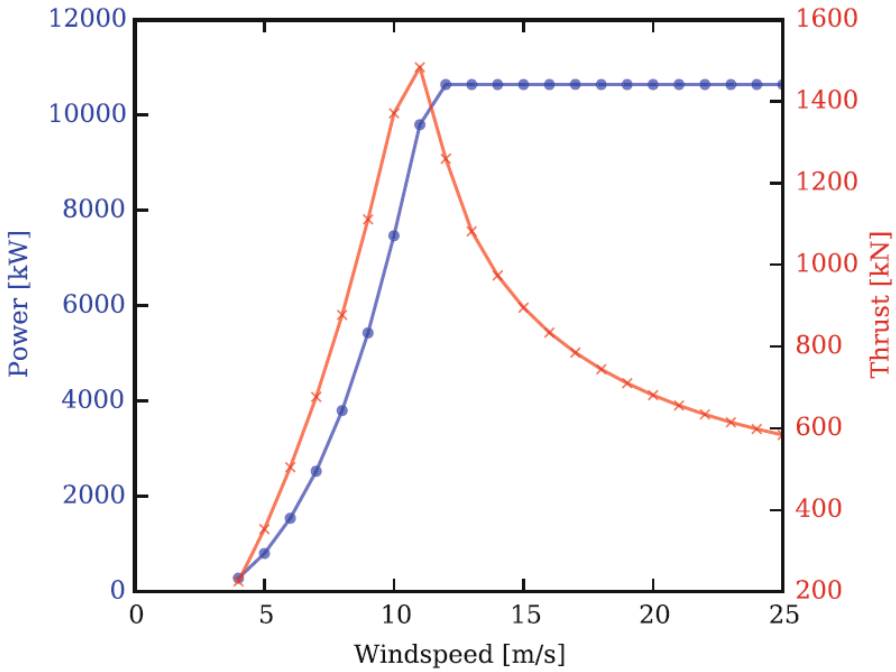

Figure 1.9: Power and thrust curve of the DTU 10 MW RWT over the operational range.

output of comparing an AWE system to an equally sized wind turbine in terms of rated power, comes at a cost: while conventional wind turbines are stationary constructions on the ground and can be stopped anytime if there is the necessity. AWE systems are much less reliable as because of their intrinsic nature: they need to fly to maintain their shape. Whenever there is a problem, an accident with major costs in terms of safety and integrity of the system may easily occur. For this reason AWE systems need sophisticated automatic controls to overcome the complexities that an intrinsically unstable and nonlinear system presents.

Basic limits about HAWE

As mentioned by Moritz Dihel in Airborne Wind Energy, there is a power limit for airborne wind energy. This limit can be achieved if the total aerodynamic force is in line with the wind direction, if the wing drag is the only loss and if the airspeed of the wing is equal to:

$$v_a = \frac{2C_R}{3C_D} v_w \tag{1.4}$$

This is a fundamental limit of how much useful power any flying body can extract from the wind field. An other limit is due to the gliding number $\frac{C_L}{C_D}$ that enters the limit quadratically: it is beneficial to have very low drag coefficient C_D. The drag caused by the tether cannot be neglected and for very efficient airfoils the tether drag can become the dominant drag contribution. For AWE systems that adopt flexible wings, usually, there is another drag that adds an heavy contribution to the total drag: the POD, which is needed for all the on-board telemetry that is useful for the autonomous control. There is still another limit that is important to remark, that is due to direction of the wind with respect to the total aerodynamic force, expressed by:

$$P_{wind} = v_w F_a cos\gamma \tag{1.5}$$

The total power P_{wind} that a flying wing extracts from this wind field is given by the product of v_w with the total aerodynamic force F_a that the wing experiences and the cosine of the angle γ between the direction of this force and the wind. Thus, in conclusion, no device can extract power in a constant wind field if it doesn't exert an horizontal component against the wind. The fact that the total aerodynamic force is not perfectly in line with the wind direction is called the *cosine loss*. Fortunately for moderate angles the cosine is still close to 1. If, for example, the tether goes upwords with an angle of 45 degrees, the cosine loss is less than 30%. The AWE companies that fly with high γ experience very high cosine losses.

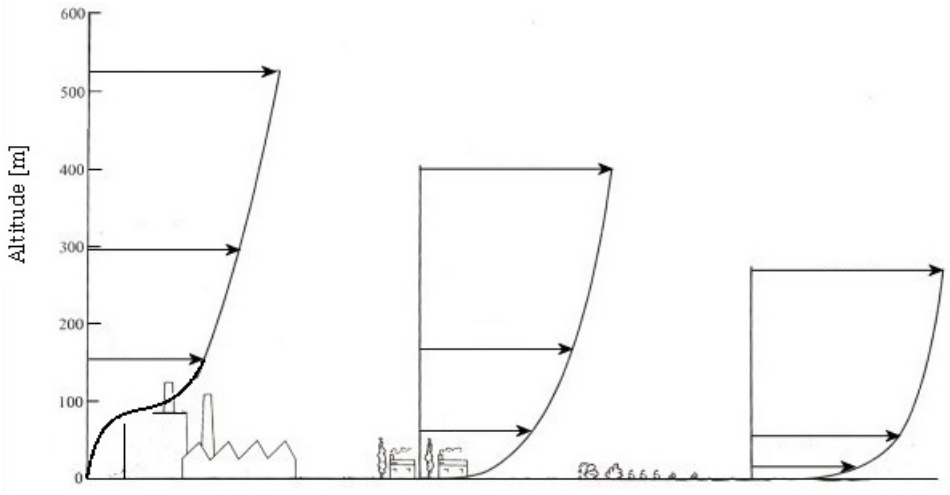

Figure 1.10: Wind speed variation compared to height from ground.

The cosine loss is related with the weight of the device that is flying but, physically speaking, gravity can be compensated with a small change in the orientation of the wing. Even if the total weight of the system would be one third of the total aerodynamic force, with a change in wing orientation of 20 degrees the cosine losses due to gravity would decrease at a mere 6%. This is the reason why gravity can often be neglected in power estimations for AWE systems.

Different strategies and approaches

Talking about AWE system it's important to have an overview of the different strategies that have been adopted worldwide in the attempt of making the AWE technology a reality. An interesting usage of the AWE principles is proposed by the German company *Sky Sails* that uses enormous kite, up to 500 m^2, to pull ships and reduce the cost of fuel propulsion. Recently, they have been investigating energy production systems to allow the AWE technology to pull ships while providing some electric power. Because the engines drive marine propellers with relevant power losses, having a kite pulling the ship while transferring some power is economically favorable. A major point of this usage of the AWE technology is that on the ships there are always a few people that are able to fix possible technical problems, which is not as common considering the typical usage of AWEs.

Another strategy concerning the usage of AWE technology is to generate directly on-board instead of having a generation system at ground level. There are a few companies that are working on this particular case but the first is the californian start-up *Makani Power*. A very significant feature of these systems is that the on-board rotors can be used for vertical take-off and landing, using the generators in motor mode. The issue of take off and landing is crucial for the AWE industry and is still a matter of investigation by all the current competitors of the market. *Kitemill*, a norwegian start-up, is currently using a hybrid prototype in term of location of the generator and take-off-landing operations. Their prototype is composed of a rigid wing that has 4 on-board turbines: thus the take-off and landing phases are handled by the on-board rotors while the generation is still a matter of ground based technologies. Various strategy in the kites design are depicted in Figure 1.11.

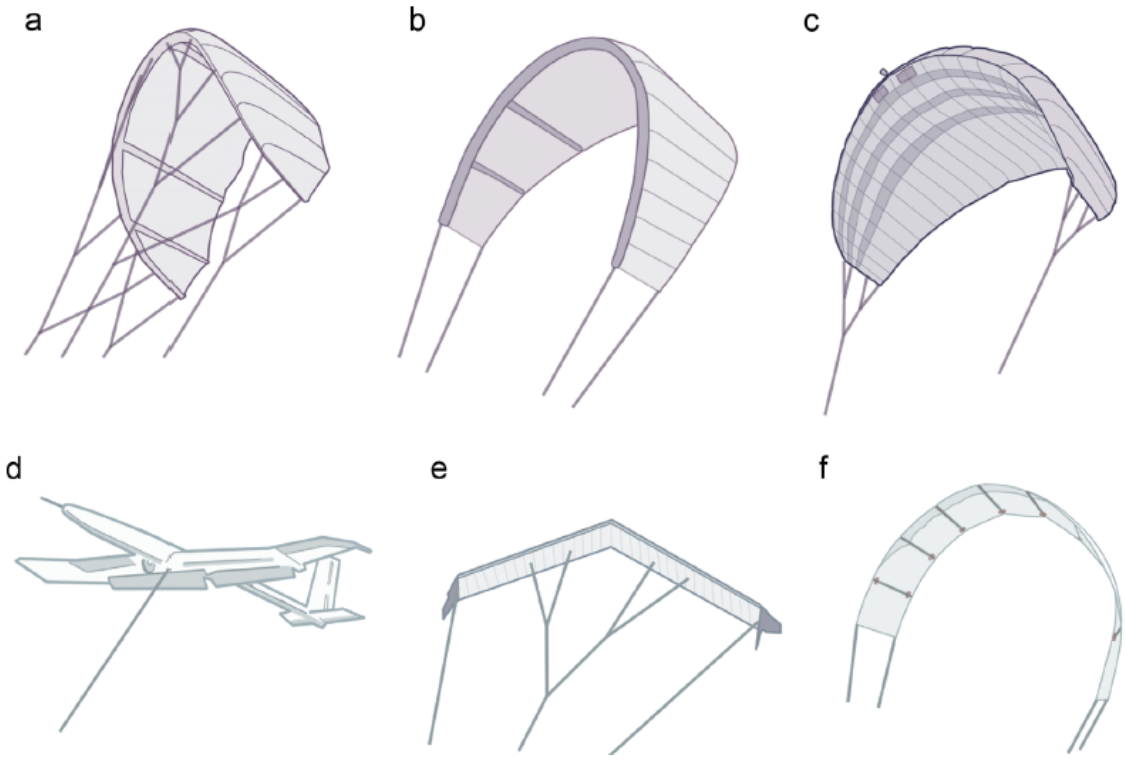

Figure 1.11: Different types of aircraft in ground generations systems. (a) LEI SLE (Leading Edge Inflatable, Supported Leading Edge) Kite; (b) LEI C-Kite; (c) Foil Kite, design from Skysails; (d) Glider, design from Ampix Power; (e) Swept rigid wing, design from Enerkite; (f) Semi rigid wing.

Since the AWE industry still leaves some space to engineering creativity, is possible to see various approaches to the problem. In this various scenario, an interesting division in the field is between soft, flexible wings that resemble surf kites or parachutes, and rigid wings that resemble airplanes. Flexible wings maintain their shape thanks to the aerodynamic load distribution generated by the air flow. They are very light systems that in case of crash do not report extreme damage to the aerostructure nor cause major damage to the impact area. Reports and experiences of on-the-field operations tend to assume that this approach is much more safe in case of humans proximity. Flexible wings, due to their intrinsic nature, presents non linear behaviour that are very complicated to control. In contrast to this, rigid wings always maintain the shape independently of the weather conditions and are usually

much more heavy. Due to their higher lift to drag ration, they reach higher velocities that are relevant for power production but may be a cause of serious damage in case of failure or crash. Nevertheless, the manufacturing cost of a flexible wing is clearly a fraction of the manufacturing cost of a rigid wing. However, a flexible wing may suffer more in terms of durability from weather conditions while a rigid wing is more tough, thus durable. An example regarding flexible wings, is presented by the italian company *Kitenergy*, that through extensive activities of research and tests on-the-field is actually working on its 60kW prototype to reach the highest levels of the TRL scale -Technology readiness levels- for the *Horizon 2020* programme.

Chapter 2

The KE-60 mkII prototype of Kytenergy s.r.l.

In this chapter the *Kitenergy s.r.l.* project is discussed. The prototype, called *KE-60 mkII*, is presented in its major subsystems along with a discussion on how it exploits high altitude wind to produce renewable and clean energy.

2.1 KE-60's evolution

Back in 2005, a team of professionals, university professors, mechanical, aerospace and automation engineers developed an innovative system to produce energy take on challenge to exploit high altitude wind to produce energy by means of a kite. initially the system was designed to fly a power kite up to $800m$ in height, than a human pilot could control it and execute the desired trajectories. Thus the control was only human. The control technique consists in imposing a certain difference in length on the kite steering cables. This delta caused a subsequent change in the shape of the kite that led to a system turn. This technology has been consolidated in four years of different tests on real scenarios. The next step was to design and build an autopilot that could fly the kite and producing energy autonomously. The system has been therefore re-designed with many sensors that have been integrated in a flying unit called *POD*, able to collect data and communicate via radio to a ground based unit all the data needed for a proper autonomous flight. A wind station has been added that could provide data on wind speed and direction at $6m$ of height: even though the wind at higher height is different, it is still related to the one almost at ground level. The challenge is on worldwide, but it is a fact: controlling a non-rigid aircraft system is not an easy task.

Today, the prototype has been totally re-designed in all its subsystems, making it one of the few prototypes in the world that can be controlled both by a human and an autopilot. The continuous interaction of the two leads in constant advancements in flight performances and in generation efficiency. The new prototype, called *KE-60 mkII*, still maintains its peculiarities: a compact device that can be easily transported and moved, providing electricity to any user, even in remote locations such as extreme North, deserts, hardly accessible mountains or islands and military camps.

2.2 Components of the system

The entire prototype is based on the continuous interaction of different subsystems that are designed and build on their specific purpose.

- the *KSU*, which stands for kite steering unit, responsible to guide the kite.
- the kite, that provides the traction needed to produce energy by flying with specific trajectories, such as the "eight". It comprehends also a specifically designed bridle system and two dyneema cables.
- the *electrical configuration*, which is responsible for the motion control and for storing the energy produced during the flight.
- the *POD*, that contains all the on-board electronics and an emergency parachute.

2.2.1 The KSU - Kite Steering Unit

The KSU is the kite's driving station, at ground level. It converts mechanical power into electrical power that may be instantly used by anyone directly connected to the prototype, a grid or a group of end users for example, or stored for later usage. The tension at ground level is sensed along with other variables such as the wind speed and direction through the usage of a weather station, and other fundamental mechanical data, which discussion is outside of the scope of this paper. In Figure 2.1 there is a view of the internal mechanics of the *KSU*, renderized. In Figure 2.2 it's possible to see the KSU's mechanics working on the field during some tests. The cables enters the KSU from the upper directional arm, that follows passively the kite's motion, then each coil is wrapped on a specific barrel which is coupled to its motor of $1900Nm$ nominal torque. More precisely, the two main electric motors are brushless, synchronous, with internal permanent magnet and can be operated in different modes. The most important are:

1. *Generation mode*, when the kite pulls unrolling the barrels. In this phase, mechanical power is converted into electrical power.
2. *Recovery mode*, in which the motors are rolling up the cables on the barrels and the kite is retracted close to the KSU to start a new generative cycle.

The *sliders* are permanent magnet, brushless servomotors of small size. They control the movement along the longitudinal axis of the KSU, by means of trailers, mainly to assure a correct winding and unwinding operation. The *pulley system* is needed to guide the cables attached to the flying kite and is patented. To brake the motion in case of emergency, some calipers may act on the discs and the systems is set to emergency mode.

In Figure 2.4 there is a photo shot on a recent mission in the military base in San Pancrazio Salentino (BR), in winter, 2017. On the back there are the electrical panels. While in Figure 2.3 there is a render of the ground station of the prototype.

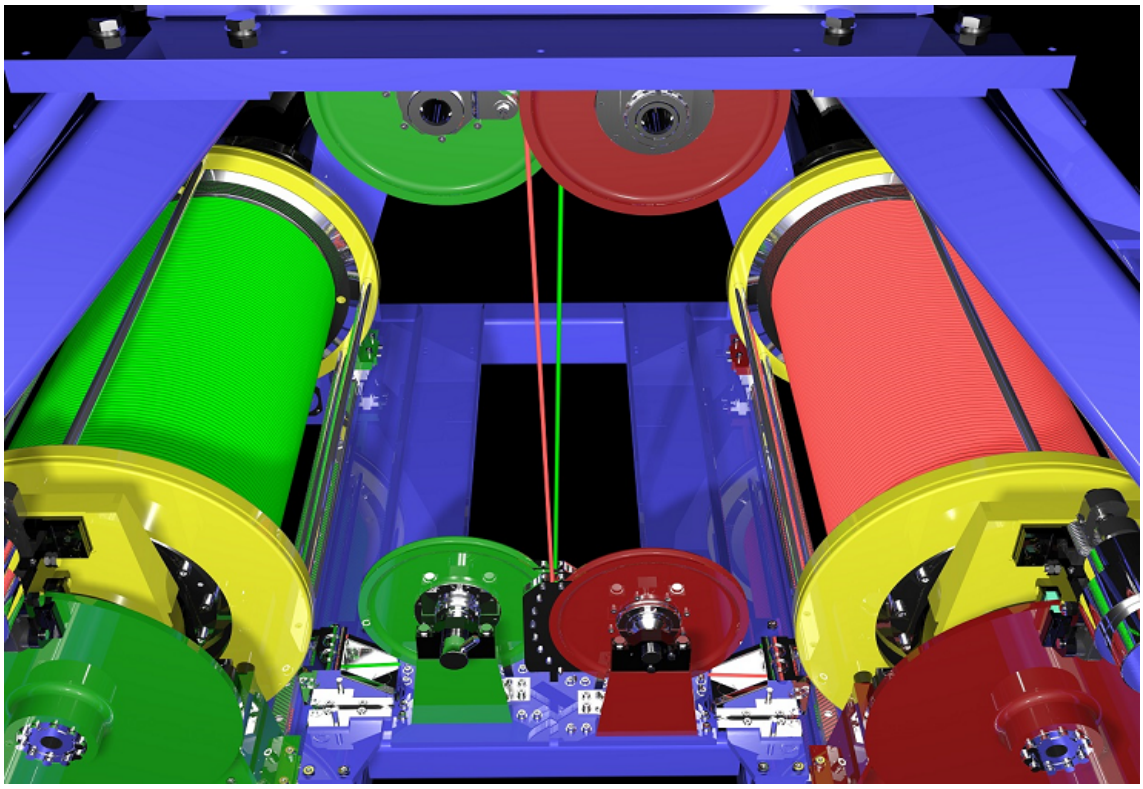

Figure 2.1: Render of the internal mechanics of the KSU.

Figure 2.2: Internal mechanics of the KSU during tests on the field.

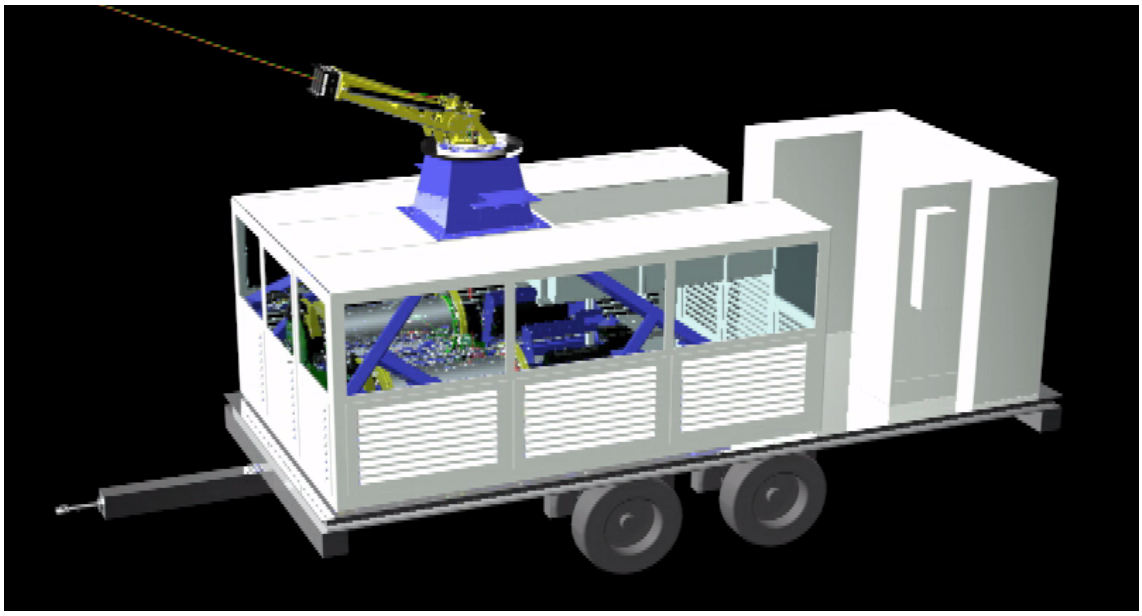

Figure 2.3: Render of the KE-60 mkII.

Figure 2.4: The KE-60 mkII on the field for some tests.

2.2.2 The kite

The power kite used by *Kitenergy s.r.l.* is of those used by kitesurfers, however it has been engineered to reach top notch performances in terms of aerodynamic efficiency. When the wind blows investing the kite interior surface, some pressure-caused forces are generated on the kite's surface. The forces have different values and direction depending on the location of the surface of the wing. In Figure 2.5 a schematic of the aerodynamic forces concentrated in the pressure center of the wing

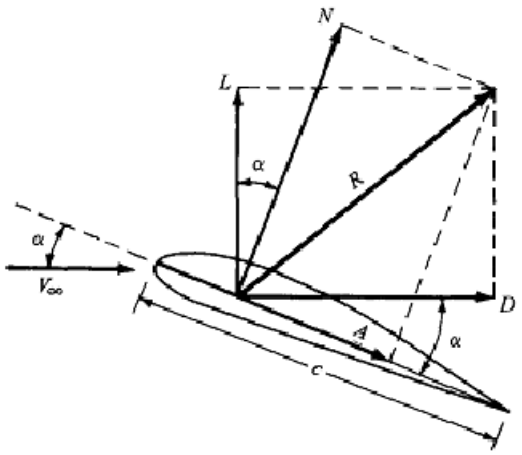

Figure 2.5: Forces acting on a kite wing section.

where D is the drag force along the wind direction and L is the lift force, which is perpendicular to the same direction. They are defined as:

$$L = \frac{1}{2}\rho S C_L V^2 \qquad D = \frac{1}{2}\rho S C_D V^2 \tag{2.1}$$

where ρ is the air density, S is the surface of the wing, C_L and C_D are respectively the lift and drag coefficients, V_∞ is the undisturbed wind speed and C is the maximum aerodynamic chord. Notice the similarity with Equation 1.2. The aerodynamic coefficients are functions of the angle of attack α. Eventually, the presence of turbulence may lead to a loss of efficiency, which is defined as

$$E = \frac{L}{D} = \frac{C_L}{C_D} \tag{2.2}$$

The other two forces depicted in Figure 2.5 are:

$$N = L\cos\alpha + D\sin\alpha \qquad A = D\cos\alpha - L\sin\alpha \tag{2.3}$$

While the force acting on the cables attached to the kite, in absolute value, is R, which is the resulting aerodynamic force.

Important factors of kite design for AWE

As mentioned before, there are various factors that should be taken into account developing a kite meant for the AWE industry.

- *Robustness*. From the sport kite, power kites need to be much more robust due to the impressive traction force they are subjected to and for the various landings.

- *Efficiency.* As defined in Equation 2.2, efficiency is dependent upon many inputs, however attention should be paid to the lightness of the anhedral arc of the primary lifting section (which is the inner third of the wing), to the taper ration at the wingtips and to the tightness of the local anhedral arc at the wingtips. This is for reducing the effects of vortices and turbulence.

- *Wingspan.* It is a matter of fact that in the AWE industry different strategies in term of airfoil geometry, besides rigid or flexible wing, may lead on very different level of system robustness and feasibility. The equilibrium between having a big wingspan, to increase power generation, and having a small wingspan, to better control and maneuver the airfoil, are thus crucial.

- *Line length.* As mentioned before, line drag is an important issue in AWE systems, thus the length of the cables should be relatively short. However long cables are needed to reach high altitude wind that are more intense and constant in speed.

- *Stability.* Since the tether and the POD presence, the center of mass is located very low below the wing, fixed in space. The wing is thus very stable with respect to the pitch and roll. In this case, the cables are also controlling lines so all turning is primarily due to yaw, but roll also contributes via a left-right asymmetry along the cables.

- *Manufacturability.* The wing should be easy to manufacture, taking into account all the sewing operations, and low cost. Thus a balance should be reached between high quality of the airfoil and affordability.

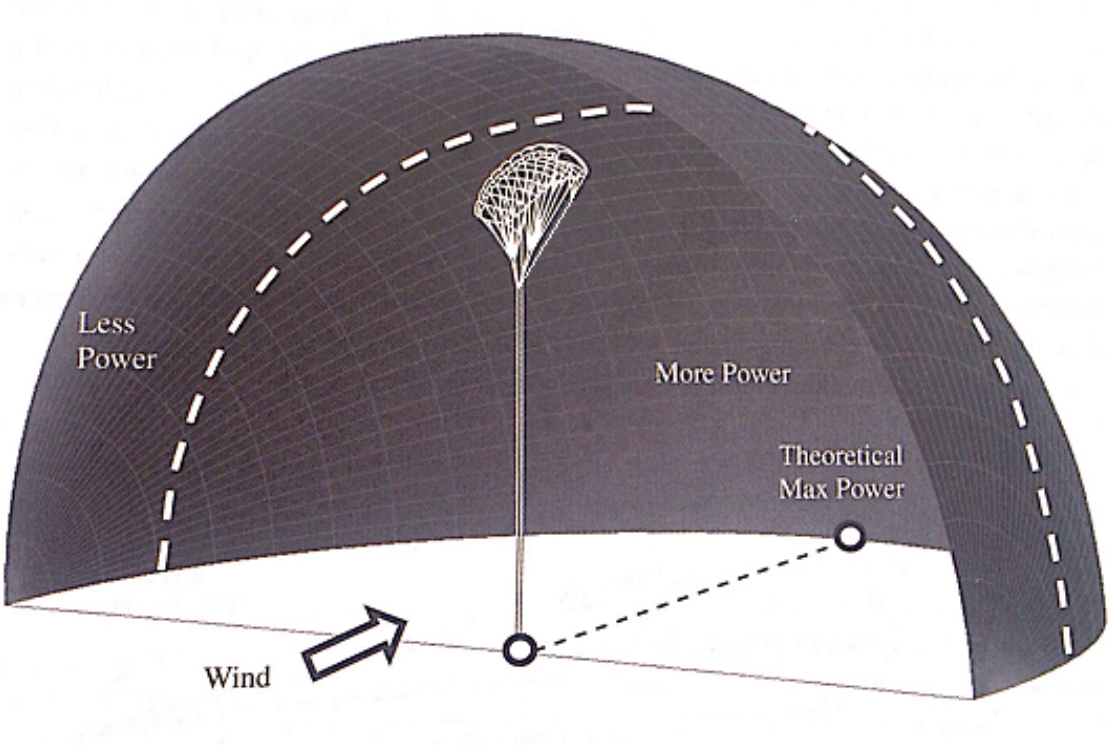

Figure 2.6: The wind window.

Cables and bridles

In Kitenergy s.r.l. prototype, the cables wrapped around the winches are made in Dyneema. These synthetic fibers are designed for traction. The diameter is $5mm$. The exceptional light weight related to the extreme high break load of this material makes these cables exceptional for the AWE industry. They are also resist very well to torsional and bending force and the elongation is also a negligible problem. Being a polymer, Dyneema is not very suitable for extremely high temperatures, but this kind of applications are out of the scope of the prototype that, anyhow, is designed to operate in extreme locations such as deserts and the extreme north.

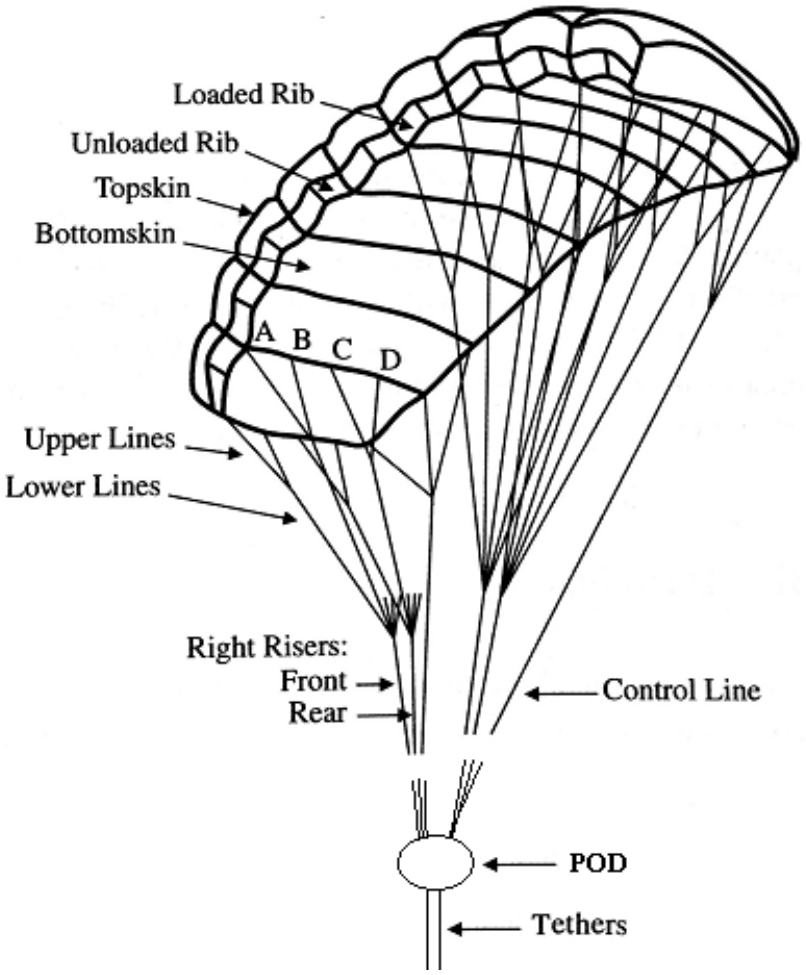

Figure 2.7: The kite.

2.2.3 The POD

The POD is crucial due to its function: transmitting data to ground. The shape has been designed to have not interfere with the fly operation, thus the aerodynamic drag due to the geometry is as low as possible. The weight also is restrained to not excessively lower the center of mass. Two wings have been designed to let the pod slide on the ground, during take-off operations. The on-board electronics are supplied with a battery, along with an on-board generation system: the on-board electronics are thus never switched off during flight and there is no need to land the kite because of low charge levels. The entire structure has been prototyped at an early stage in polylactic acid, a biodegradable, thermoplastic polyestered derived from renowable sources that is often used in rapid prototyping along with 3D printing technologies. The structure, then, has been printed in ABS, which is a petroleum based polymer that has excellent mechanical characteristics that match correctly with the POD usage. As a flying device, the POD has been equipped with an emergency system, a brake element such as parachutes, that is able to land safely the POD in the remote case of a kite total failure.

A metal-made ferrule is attached directly to the load lines, transmitting the forces through the parts of the system. Considering that the kite steering is actuated at ground level by means of a delta in the length of the cables, is very important to have a back-up system that is able to properly estimate the different lengths. Thus, the POD's on-board electronics include an encoder and some infrared sensors to monitor the movements of the cables, some GPS and various IMU and gyroscopes. However, is also important to know the local pressure, thus this functionality has been added to the system. A system able to sense the tension on the bridles has also been deployed an integrated in the aerostructure. Since the system must be able to avoid total failure in case of ground impact, an anti-shock layer covers the inside of the rigid structure while the internal redundancy significantly increases the safety and reliability of the POD-related operations.

2.2.4 The electrical configuration

The actual electrical system has been designed and realized to achieve the best industrial standards, thus is reliable and robust. The entire electrical system has to be considered as the interaction of the power conversion subsystem and the storage subsystem.

Storage system

Since the battery pack alone is not able to store energy properly, a bank of supercapacitors has been added. The supercapacitors have a high dynamic behaviour and by working along with the batteries a synergy can be achieved and energy stored in all cases. The batteries used in the KE60 are of AGM type. Between the pros it's important to remember that they are not so inclined to sulfatation and are robust to low temperatures, spill proof, can be deeply discharged, hermetically sealed, they can be charged very quickly and their lifespan is generally considered longer if compared to other kinds. On the other side they are expensive, heavy and electrically asymmetric, thus the need to add supercapacitors. The battery adopted in

the KE60 are able to supply the entire system in case of maintenance. The supercapacitors have been introduced to safely and efficiently manage the maximum power conditions as wind gusts.

Power conversion

In Figure 2.8 the actual electrical configuration is shown. The prototype in its actual configuration is rated for a nominal power of $60kW$. The storage system is connected to a DC/DC converter able to transfer a maximum continuous current of 260A. The batteries and supercapacitors discussed previously are here shown, along with the two slider motors and torque motors. The DC bus is maintained at 600V.

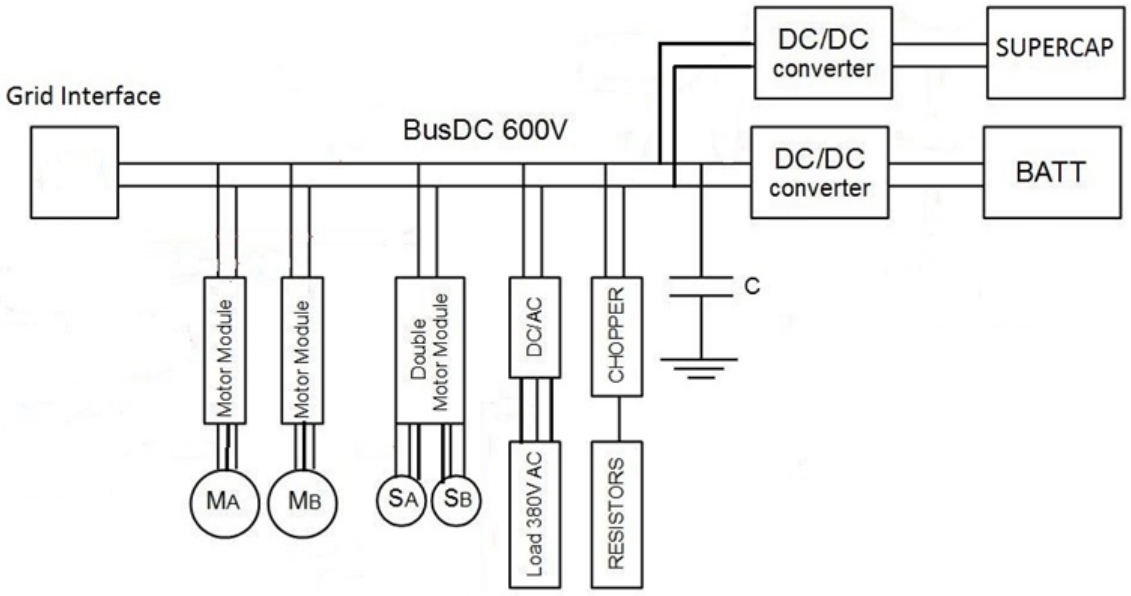

Figure 2.8: The electrical configuration.

2.3 Operation phases

As shown in Figure 1.10 the kite has to fly in downwind direction in order to maximize power. All the operations may be considered as part of the generation cycle that is also called *yo-yo*. In the yo-yo cycle two different phases can be considered. The first one is surely the generation phase while the second one is the recovery phase. During generation, the kite is flown along a specific trajectory that, in this case, is called the *bang to bang* trajectory. In this case, the path is similar to an eight shape and the kite can fly always as downwind as possible, without twirling the cables. Considering a $1000m$ cable and a wind of $15m/s$, the cables should be

unrolled around $5m/s$, thus the generation phase can last $200s$. The recovery phase may last between $50s$ and $200s$ depending on the chosen technique. With a constant traction of $12000N$, the power output is $60KW$ every cycle. The generated energy amount is therefore:

$$E = 60kW * 200s = 12000kJ \tag{2.4}$$

However the recovery phase absorbs around $7kW$. The worst energetic case is then

$$P = 7kW * 200s = 1400kJ \tag{2.5}$$

thus the usable energy is

$$E = 12000kJ - 1400kJ = 10600kJ \tag{2.6}$$

The best energetic situation is characterized by a shorter recovery time, so

$$P = 7kW * 50s = 350kJ \tag{2.7}$$

The usable energy, therefore, is

$$12000kJ - 350kJ = 11650kJ \tag{2.8}$$

In the worst case, an entire cycle lasts $200s + 200s = 400s$. Considering that $3600s/400s = 9$, the total produced energy is

$$11650kJ * 9 = 95400kJ \tag{2.9}$$

with an average power of

$$95400kJ/3600s = 26.5kW \tag{2.10}$$

In the best case, an entire cycle lasts $200s + 50s = 250s$. Taking into account that $3600s/250s = 14.4$, the total produced energy is

$$11650kJ * 14.4 = 167760kJ \tag{2.11}$$

with an average power of

$$167760kJ/3600s = 46.6kW \tag{2.12}$$

Since Kitenergy S.r.l. has designed, tested and developed different strategies to reduce the recovery time up to $50s$, relevant energetic performances have been enhanced.

2.3.1 Generation phase

The generation phase, also called *traction phase*, generally lasts for 200s. The kite is as perpendicular as possible with respect to the wind direction in order to maximize power. The kite moves away from the KSU making eight shaped orbits, pulling the cables and converting mechanical power into electrical power. A suitable breaking torque is imposed according to the unrolling speed. The generation phase ends when the maximum length of the cables is reached. In Figure 2.9 the generation phase is shown, while in Figure 2.10 the power flow during generation is shown.

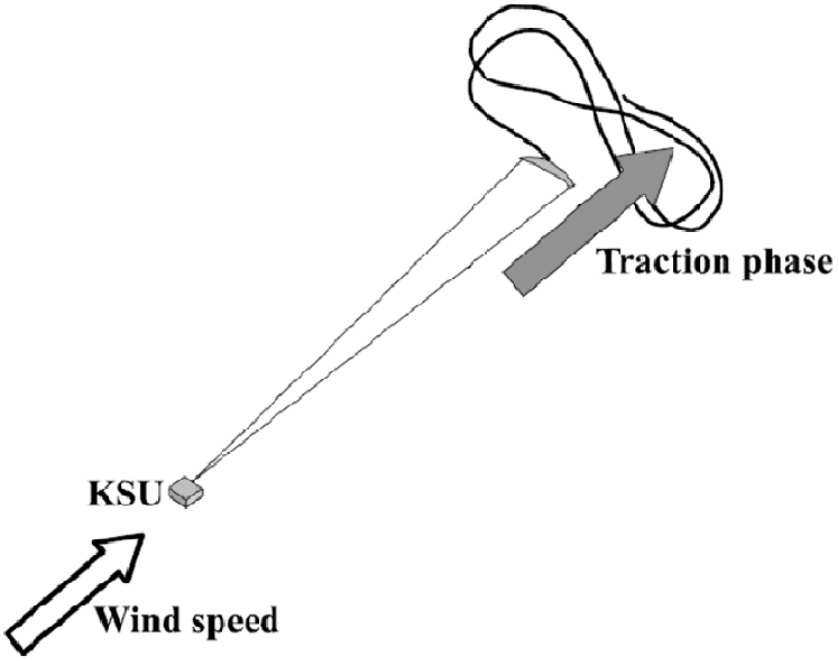

Figure 2.9: Generation phase.

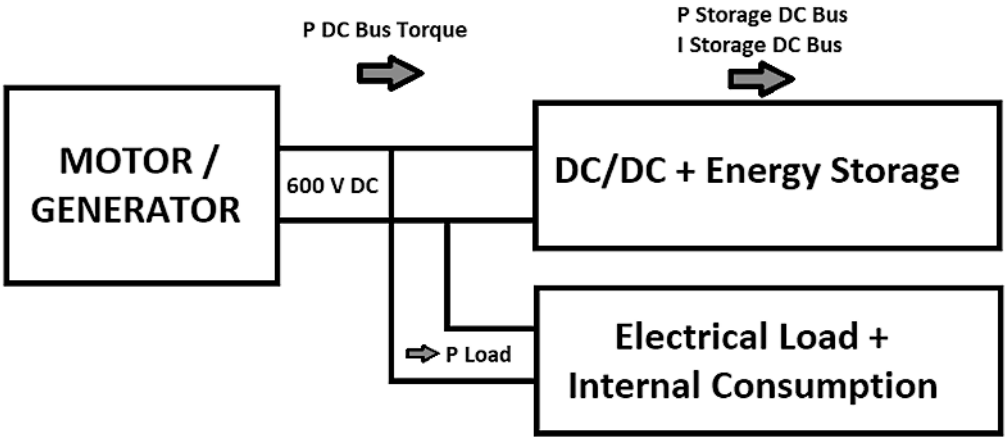

Figure 2.10: Power flow during generation.

2.3.2 Recovery phase

The recovery phase begins as the generation phase ends. The kite is pulled back again close to the KSU. in order of limiting the power consumption of this phase, various techniques have been developed. Here one is depicted in Figure 2.11 in which the kite is driven in a lateral zone from the wind window so that it remains swollen enough to be safely controlled but still develops little bearing. In this phase, electrical power is converted into mechanical power as shown in Figure 2.12. Once the cables have been rolled on the winches and the kite is in an adequate position, a new cycle begins and a new generation phase starts.

The continuous alternation between generation and recovery phase doesn't allow a defined duty cycle, so it's necessary to refer to average values that are statistically more likely to occur.

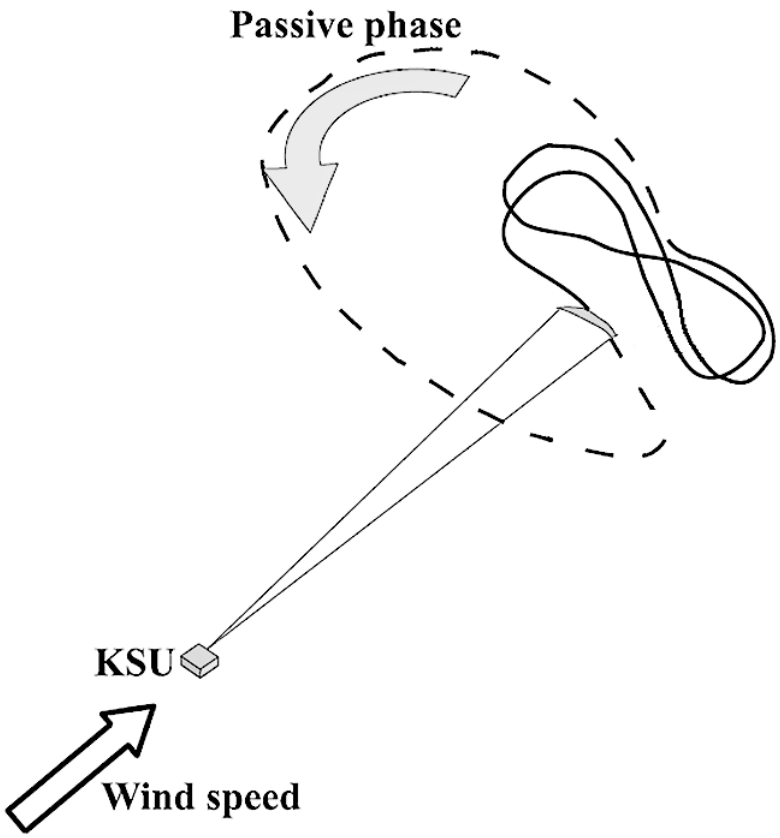

Figure 2.11: Recovery phase.

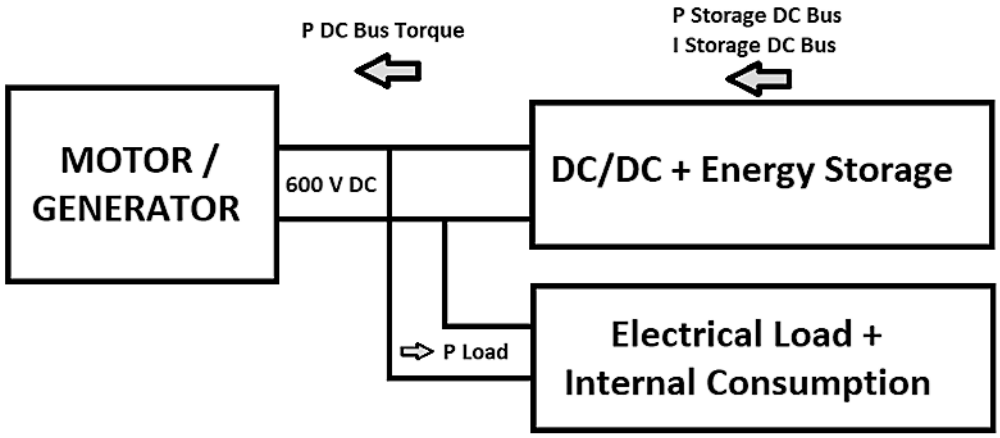

Figure 2.12: Power flow during recovery.

2.4 On-the-field-testing

The technology has been tested in several Italian locations. For all these test campaigns, Kitenergy s.r.l. carefully focused on relationships with the institutions responsible for control and management of the airspace: National Authority for Civil Aviation (ENAC), National Agency for Air Navigation Services (ENAV), Air Force (AM) with the goal of ensuring the maximum safety and integration with the existing rules and regulations.

The various campaigns have been fundamental for the actual prototype's configuration, that is closer than ever to a feasible industrial product. The various

test sites range from mountain terrain to offshore land: Usseaux(TO), Ascoli Satriano(FG), Verrayes(AO), Solarussa(OR). The last campaign took place in San Pancrazio Salentino(BR) in a military base. In Figure 2.4 the prototype is operating on the field for some tests.

Chapter 3

Traction sensing system

This chapter is about the design and development of the traction sensing system. The circumstances that were the base to develop this technology are here presented, along with the sensors available on the market that have been used. The electronic schematics, made in Eagle, are shortly presented in order to show how the sensors are connected with the rest of the avionics. The sensor characterization is then discussed showing the methodology adopted, the data analyzed and collected in both compression and traction tests. Finally, the integration of the sensing system is briefly presented.

3.1 The problem

Correctly sensing and monitoring the traction forces on a kite wing or, eventually, on a rigid wing, is crucial. This is because understanding how the wing inflates, it's behaviour along the entire flight cycle and how its aerodynamic behaviour changes in time helps maximizing the mechanical power that is possible to extract from the wind. Furthermore, understating the dynamic of the forces along the wing is fundamental to improve the characteristics of the aerostructure.

3.2 Traction and compression sensor

Considering the circumstances, a loadcell is the kind of sensor that better match all the needs. Specifically, the loadcell comes from a German manufacturer, *Batarow Sensorik GmbH*. The sensor code is *MB631*, rated for 8kN of capacity. The dimensions and technical drawings are shown in Figure 3.1 and in Figure 3.2.

Considering the fact that the POD has to fly 24h in almost any weather condition, the IP 64 or above protection class established an asset in the identification process. The other asset has been the capacity factor: 8kN is a reasonable value taking into account that the entire kite system pulls up to 1.5 tons. The overall dimensions where as important as the parameters discussed above because the loadcell had to be installed onboard the POD, through the holes of a metal gear that had been previously drilled to obtain the housing for the loadcells. The specifications of the single load pin are listed in Table 3.1, but it's important to remark that the project is designed with six loadcells.

MB 631-8 load pin	
Parameter	Value
Material	Stainless steel
Protection class	IP 64
Capacity	8 kN
Safe load limit	9.6 kN
Breaking load	16 kN
Rated output	1 mV/V
Zero balance	0.05 mV/V
Exitation	10 V
Input resistance	1200±200 Ohm
Output resistance	1002±2 Ohm
Insulating resistance	>5 GOhm
Precisionclass	1%
Nonlinearity	±40 N
Non repeatability	±20 N
Hysteresis	±16 N
Temp. shift zero	±4 N/K
Temp. shift span	±4 N/K
Compensated temp.	-10 ... +60 °C
Operating temp.	-20 ... +70 °C

Table 3.1: Specifications of the MB631 load cell.

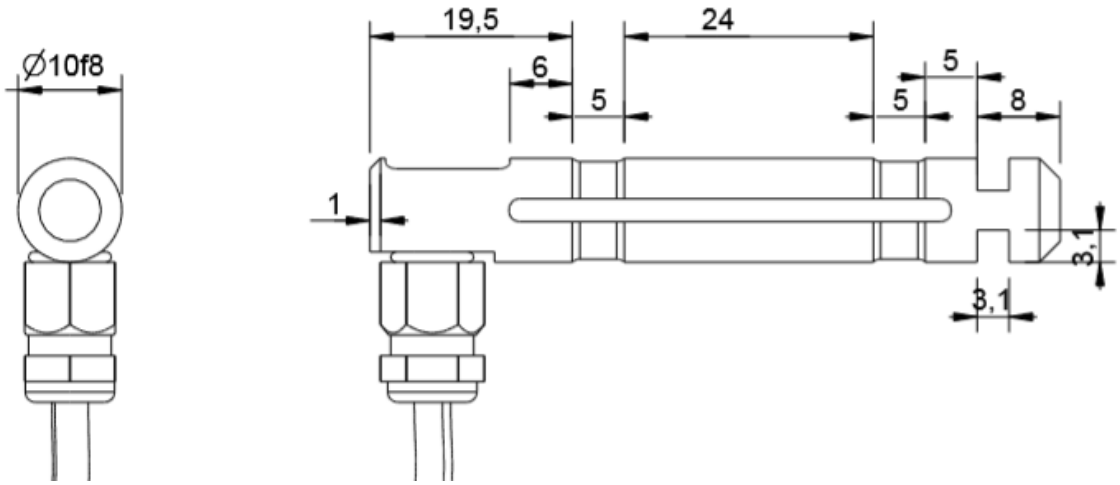

Figure 3.1: MB631 load pin technical drawing.

The output of the MB632 has to be considered as positive under compression forces while negative under tension forces: these cases have to be referred taking into account the orientation of the loadcell as depicted in Figure 3.3. Since this sensor is not tri-axial the forces have to be applied as perpendicular as possible with respect to the longitudinal ais of the loadcell. Otherwise, if the force is applied with a certain angle, the loadcell will detect only the component of the force that is perpendicular to its axis.

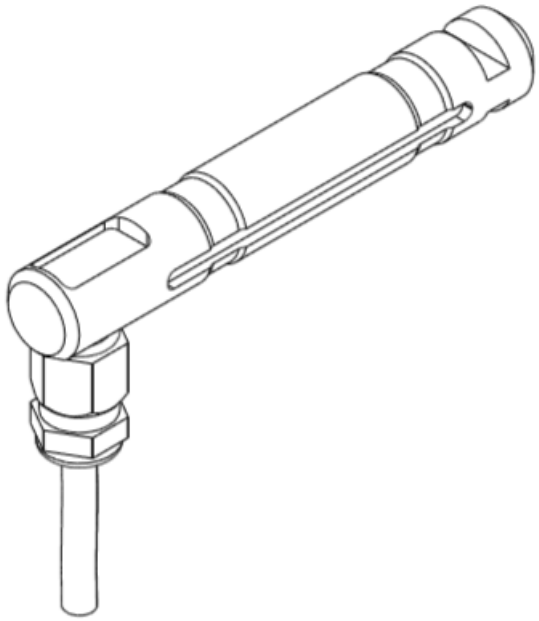

Figure 3.2: MB631 load pin technical drawing.

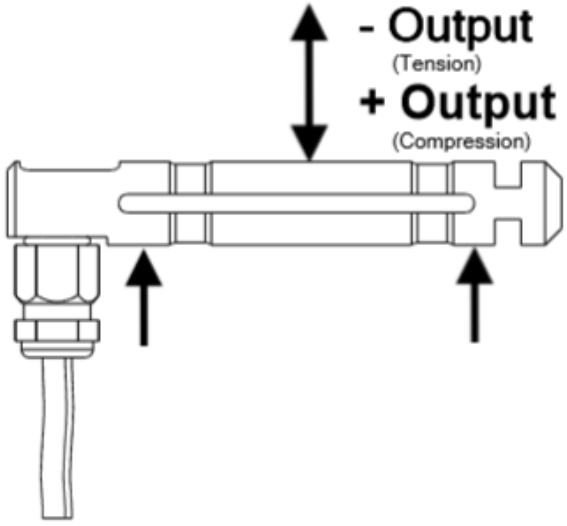

Figure 3.3: MB631 output schematic.

3.3 The INA125

To properly supply one loadcells with 2.5V and amplify the signal before the microprocessor, an operational amplifier with precision voltage reference has been used. The operational amplifier is, in this case, the INA125 from *Texas Instruments Incorporated*.

3.3.1 Schematics

The INA125 provides complete bridge excitation and precision differential-input amplification on a single integrated circuit. Since it came in 16-pin plastic DIP and SO-16 surface-mount packages and since it is specified for the –40 Celsius to +85 Celsius, which is perfect for the POD final usage while fitting into the industrial temperature range, the INA125 is extremely useful for rapid-prototyping while still

being suitable for a final industrial design. The voltage reference was externally adjustable with pin-selectable voltages of 2.5V, 5V, or 10V. The 2.5V has been selected as the right pseudo-ground. The reference voltage is accurate to ±0.5% (max) with ±35 ppm/Celsius drift (max). Finally, a sleep mode allows shutdown and duty cycle operations to save power and a single external resistor sets any gain from 4 to 10,000. In Figure 3.4 it's possible to see the schematic used in the project while in Figure 3.5 there is the part of the PCB project onboard the POD with the six INA125 connected.

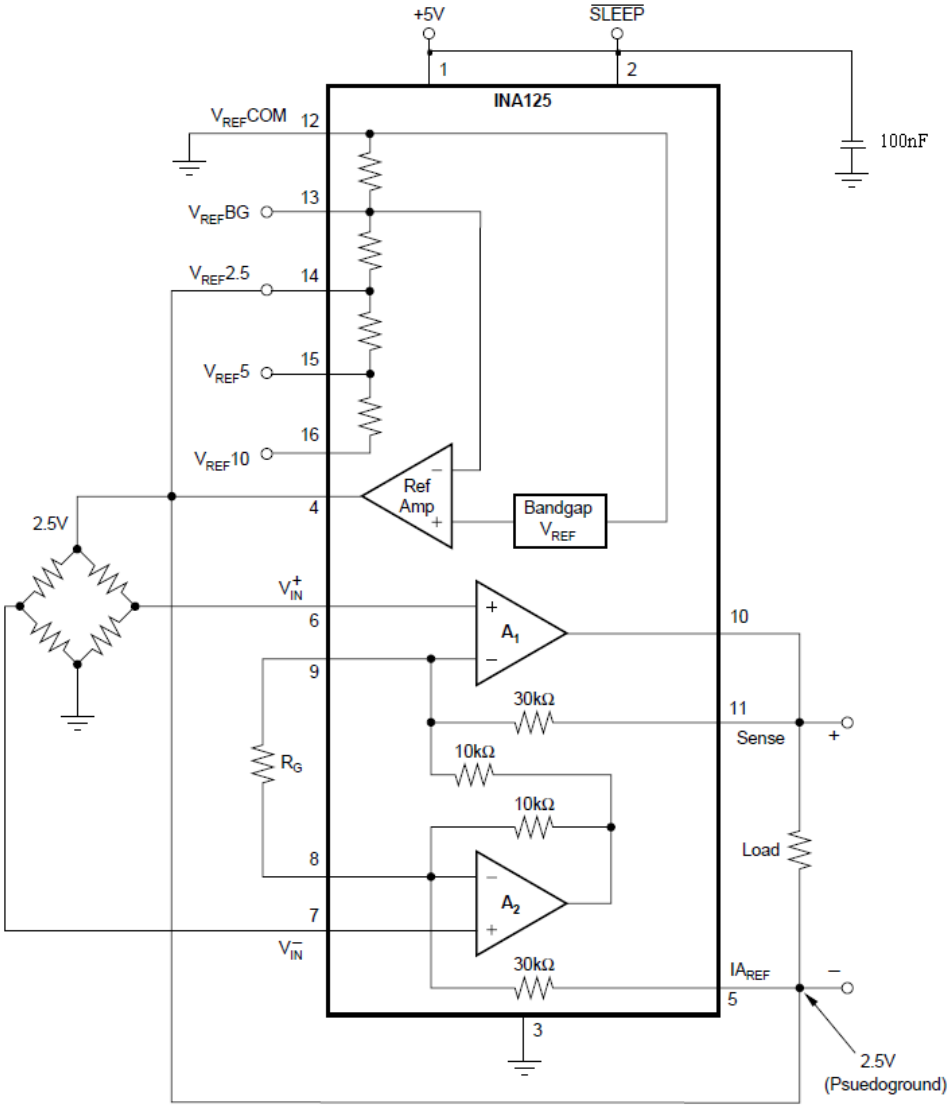

Figure 3.4: Configuration and schematic designed for the INA125.

The inputs of the INA125 are individually protected for voltage up to ±40V. For example, a condition of –40V on one input and +40V on the other input will not cause damage. Internal circuitry on each input provides low series impedance under normal signal conditions. To provide equivalent protection, series input resistors would contribute excessive noise. If the input is overloaded, the protection circuitry limits the input current to a safe value of approximately 120μA to 190μA. The inputs are protected even if the power supplies are disconnected or turned off: this is important in the case of a flight fail, even though the chances are very low.

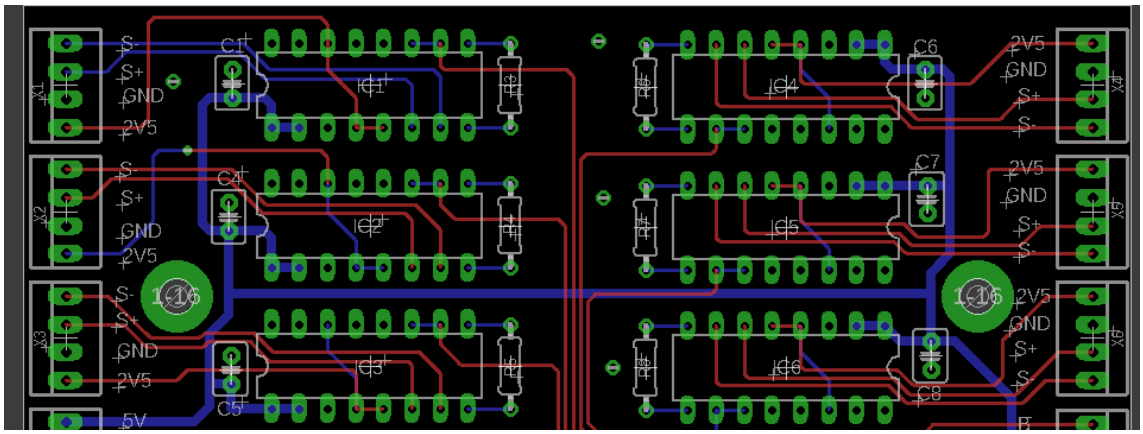

Figure 3.5: The six INA125 on the PCB, made with Eagle.

3.3.2 Setting the Gain

The Gain of the INA125 is set by connecting a single external resistor, R_G, between pins 8 and 9 son that

$$G = 4 + \frac{60k\Omega}{R_G} \tag{3.1}$$

Considering that a Gain of 500 is suitable for the project, by setting $G = 500$ and reversing the formula, R_G is

$$R_G = \frac{60k\Omega}{G - 4} = 121\Omega \tag{3.2}$$

which is also the nearest 1% value in real resistors in Ohm. The output, at this point called V_O, is on the load between pins 11 and 5, so that

$$V_O = +2.5V + G(V_{IN}^{+} - V_{IN}^{-}) \tag{3.3}$$

which is connected to the microcontroller for data acquisition and analysis purposes.

3.4 Sensor integration

First the loadcells have been inserted into the various mounting holes on the metal gear of the POD. The loadcells have been located strategically on the metal gear, in order to have a proper tension distribution on the surface while keeping all the bridles separated from each other. Since the loadcells are located on an almost circular surface, correctly testing and characterizing the sensors requested a specific loadcell orientation. It's important to remember that a single loadcell is able to read only the perpendicular component of the force acting along its longitudinal axis. For this only purpose, some plates where designed and produced via 3D printing technology in PLA. The plates have been inserted into the metal gear immobilizing the loadcells and fixed with a M3 screw, preventing a rotation of the sensors that could alter the measurements. The contact area beetween the loadcells and the printed plates is visible in Figure 3.1 on the right: it is an engraved cut 3.1 mm deep and 3.1 mm wide.

At this point the loadcells are linked to the bridles through screw-type connectors and mechanical tosts. In Table 3.2 the mechanical characteristics of the different tosts are shown while in Figure 3.6 it's possible to see some tosts. The single-insert tosts have a round hole, the reserve-insert tosts have an oval hole. Usually, for a safety concern, the two cables used to steer the kite are connected to the POD via tosts: one cable has a very high breaking point tost-system while the other is designed to be breakable. In this way, in case of danger, one of the tost breaks and the kite cannot fly around uncontrolled because of the last cable: the kite will land safely and relatively slowly.

Tosts breaking loads		
Insert n.	Coulour	Breaking load
1	Black	1000±100 kg
2	Brown	850±85 kg
3	Red	750±75 kg
4	Blue	600±60 kg
5	White	500±500 kg
6	Yellow	400±40 kg
7	Green	300±30 kg

Table 3.2: Tosts mechanical characteristics.

To avoid a possible motion of the screw-carabiner on the fixed loadcell, some spacers have been designed and build via 3D printing in PLA. In Figure 3.7 it's possible to see the spacers and in Figure 3.8 it's possible to see some technical drawings of the plates used to fix the various loadcells. The PLA is very useful for rapid prototyping since it's very light, cheap and if the various parameters are properly set before the printing, the outcome may also be of a relative high quality and robustness.

Figure 3.6: Various tosts.

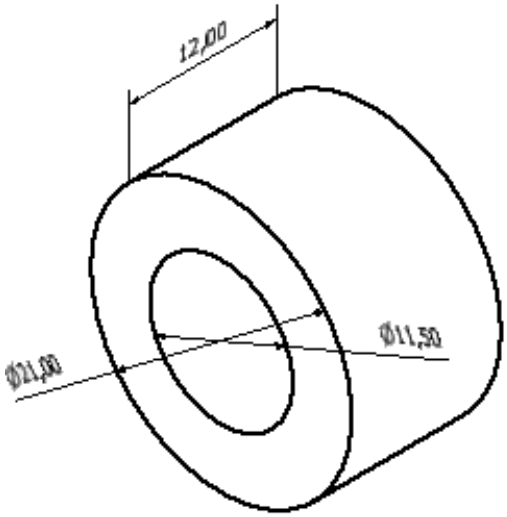

Figure 3.7: Spacers 3D printed in PLA.

3.5 The test-bench

A test-bench has been designed and build under specific criteria, such as

- relatively cheap
- small in overall dimensions
- light, but still able to load hundreds of kg
- safe
- robust

For this purpose a lat-machine has been chosen. The lat-machine has been modified allowing the POD to be hanged, thus the loadcells could be tested with compression and traction forces. In Figure 3.9(a) the original lat-machine is shown. To achieve the requested characteristics for the test-bench, some modifications have been implemented. The modified lat-machine is visible in Figure 3.9(b) in which the structure is anchored to the wall and the squared section beam has been secured -even if it's

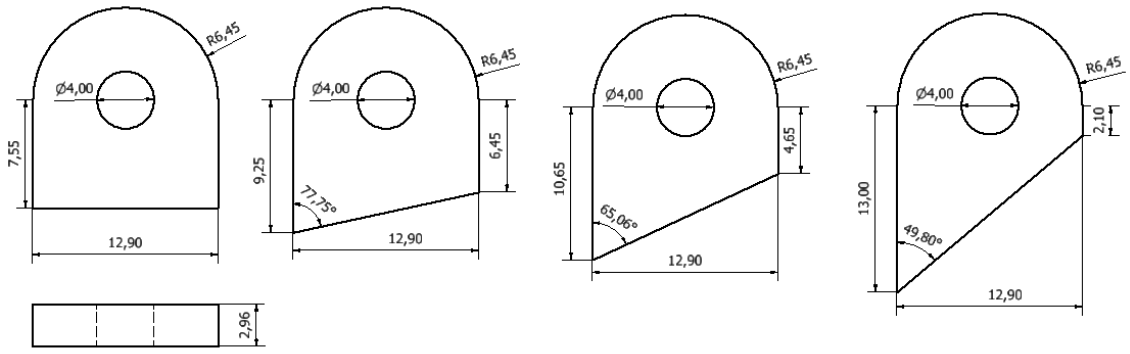

Figure 3.8: Plates 3D printed in PLA.

not valuable in the picture- to prevent bending by inserting some metal reinforcements in the points of maximum load. Some modifications have been applied also to the pulley system, as visible in the picture. In Figure 3.9(c) the used test-bench is depicted: the POD hangs from the beam by means of a pulley, a swivel and a 900 kg screw-carabiner that are linked through a 600 kg tost to the load cell. The POD system is anchored to the ground to oppose a necessary resistance to the load. In this way the POD is simply lifted by the load while the loadcell is able to sense the tension.

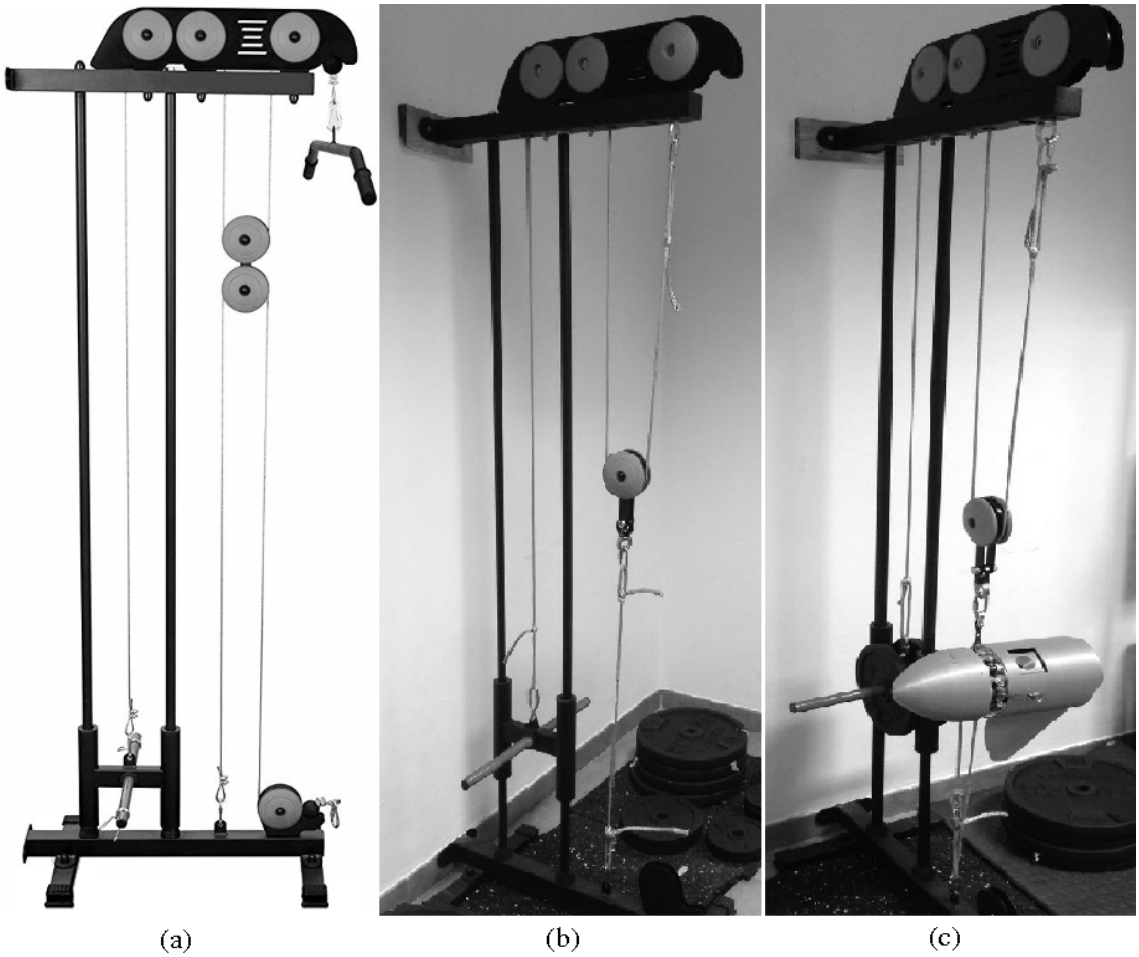

Figure 3.9: The various stages of the test-bench.

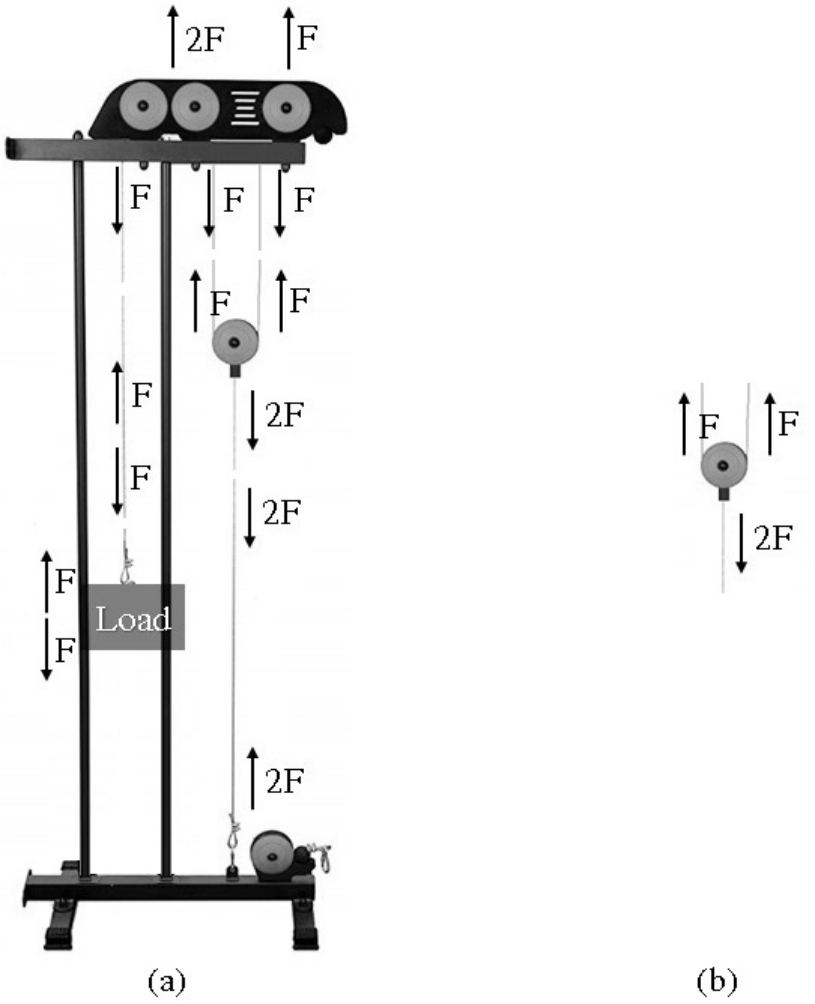

Figure 3.10: Tension distribution on the cables.

In Figure 3.10(a) it's possible to see the modified lat-machine. A load is applied in order to produce some tension on the pulley on the right. The POD hangs just under it, as depicted in Figure 3.9(c). Since the POD is positioned as described, if a load F is applied, the POD will be subjected to a load 2F, as the schematic in Figure 3.10(b) describes. Therefore, if the load is, for example, 5 kg, the POD is subjected to a 10 kg load. Fore safety concerns, the work-bench has been tested with 200 kg as a maximum load, which means that the load cells have been tested with 400 kg load in both traction and compression.

3.5.1 Traction test

In Figure 3.11 the configuration adopted for the traction test is shown. There are three loadcells in the picture but only the one in the center is actually under load. The test is done by first reading the offset, then some weight is progressively added on the lat-machine and the data output from the microcontroller is analyzed. Once reached 200 kg on the lat machine, the weights are progressively discharged with an opposite sequence. Adding A, B and C as loads, means that when discharging the loadcell by removing the weights, the right sequence is C, B and finally A. For each weight, 10 measurements have been taken and the mean value has been set as the real measurement. The entire process is done for every loadcell, one after the other.

Figure 3.11: Traction test set up.

3.5.2 Compression test

In Figure 3.12 the configuration adopted for the compression test is shown. There are three loadcells in the picture but only the one in the center is actually under load. The test is done exactly in the same way as the *Traction test*. The only main difference is that the loadcells are mounted on the metal gear upside-down.

Figure 3.12: Compression test set up.

3.6 Data analysis

3.6.1 Offsets

In the tables below different offsets are reported. Each loadcell, which is characterized by a specific ID number, has been tested with zero load on a different INA125.

Loadcell n. 17104283		
INA125 n.	Load $[kg]$	Offset $[mV/V]$
1	0	71
2	0	73
3	0	75
4	0	70
5	0	65
6	0	78

Table 3.3: Offsets on Loadcell n. 17104283.

Loadcell n. 17104290		
INA125 n.	Load $[kg]$	Offset $[mV/V]$
1	0	72
2	0	74
3	0	82
4	0	90
5	0	85
6	0	88

Table 3.4: Offsets on Loadcell n. 17104290.

Loadcell n. 17104288		
INA125 n.	Load $[kg]$	Offset $[mV/V]$
1	0	70
2	0	73
3	0	84
4	0	88
5	0	82
6	0	78

Table 3.5: Offsets on Loadcell n. 17104288.

It's important to note that a single loadcell is not meant to have a zero output when no weight acts on it. The different signals of the various loadcells are received in the microcontroller of the POD at the ADC, thus an approximation error is also introduced. However, considering the usage of the sensor, the typical weights acting on the loadcells in daily operations and the the entity and magnitude of this approximation, the error has been considered negligible.

Loadcell n. 17104287		
INA125 n.	Load $[kg]$	Offset $[mV/V]$
1	0	75
2	0	86
3	0	82
4	0	76
5	0	91
6	0	77

Table 3.6: Offsets on Loadcell n. 17104287.

Loadcell n. 17104282		
INA125 n.	Load $[kg]$	Offset $[mV/V]$
1	0	81
2	0	75
3	0	73
4	0	77
5	0	80
6	0	81

Table 3.7: Offsets on Loadcell n. 17104282.

Loadcell n. 17104286		
INA125 n.	Load $[kg]$	Offset $[mV/V]$
1	0	78
2	0	97
3	0	75
4	0	80
5	0	83
6	0	92

Table 3.8: Offsets on Loadcell n. 17104286.

Thus Q is the resolution of the ADC and it's equal to its LSB, while E_{FSR} is the full scale voltage range, calculated as

$$E_{FSR} = V_{Ref}^{Hi} - V_{Ref}^{Low} = 3.3V \tag{3.4}$$

knowing that the ADC is 12 bit resolution based, so M = 12, the quantization levels are

$$2^M = 4096 \tag{3.5}$$

therefore the ADC voltage resolution is

$$Q = \frac{E_{FSR}}{2^M} = \frac{3.3}{4096} = 0,00080V \tag{3.6}$$

The correct proportionality between mV/V and kg has been tested and verified in order to proceed with traction and compression tests. In Figure 3.13 it's possible to compare the data acquired via a digital multimeter in laboratory with the data acquired in the exact same instant via Simotion. All the curves have been shifted of 2.5V because of the presence of the pseudoground, due to the configuration discussed in Figure 3.4 that leads to a V_O described in Equation 3.3. The curves are to be considered as almost overlayable.

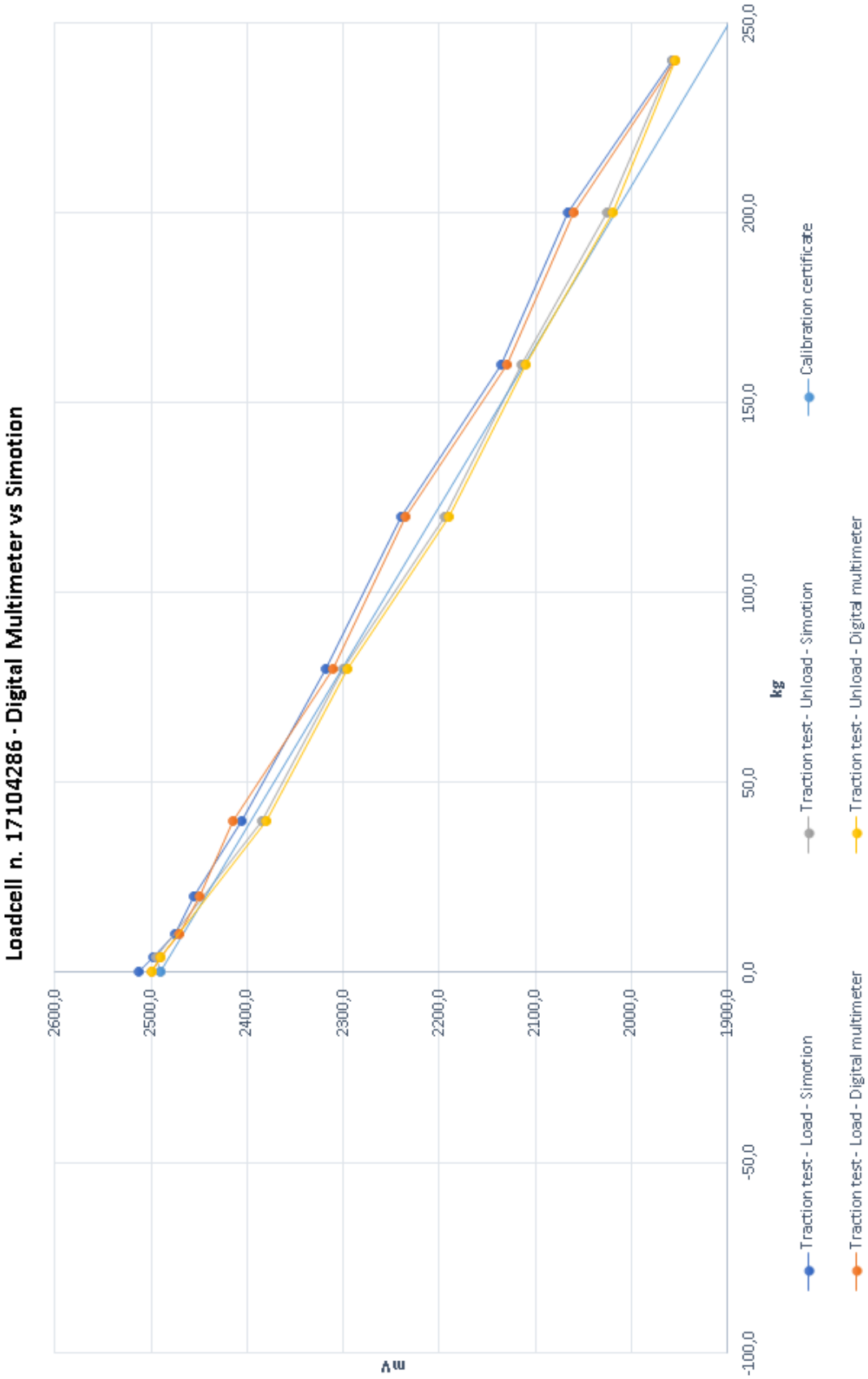

Figure 3.13: Traction test output on load cell n. 17104286, data acquired with Simotion and with a digital multimeter.

3.6.2 Test results

Here the results of the various tests are shown. In Figure 3.14 the compression test in both load and unload conditions is shown along with the traction test in load and unload conditions. The lines differ from those of the calibration certificate: this is caused by the presence of the offsets that shift the values. Since the motion control is Siemens based, the different offests have been managed not in the microcontroller of the POD, but instead at ground level, in *Simotion*. This specification has also been driven by the long term vision in which a commercial product should have most of the important logic implemented in Simotion.

In Figure 3.15 it's possible to see on the same graph the outputs of the same test conducted in Figure 3.14, with the exception that in this case the data have been acquired directly throughout Simotion, managing the offsets. The load and unload cycles show a good linear behaviour and they stick reasonably well on the calibration certificate. It should be kept in consideration that using negative weights is impossible, so the data on the third quadrant have been mirrored to obtain a more intuitive graph. The graphs show a almost hysteresis-free behaviour. In Figure 3.16, Figure 3.17, Figure 3.19 and Figure 3.20 it's possible to see the test results of the other loadcells. The tests demonstrate that the loadcells have been successfully configured and integrated into the data transmission chain. Even though some data seems to be slightly detached from the main behaviour, all the loadcells reasonably follow the calibration certificate. The test have been conducted adding various disk weights to the lat-machine, thus it's possible to say that this step response is probably not the best way to test the sensors, but still it's probably the only one that could successfully respond to the criteria set for the test-bench.

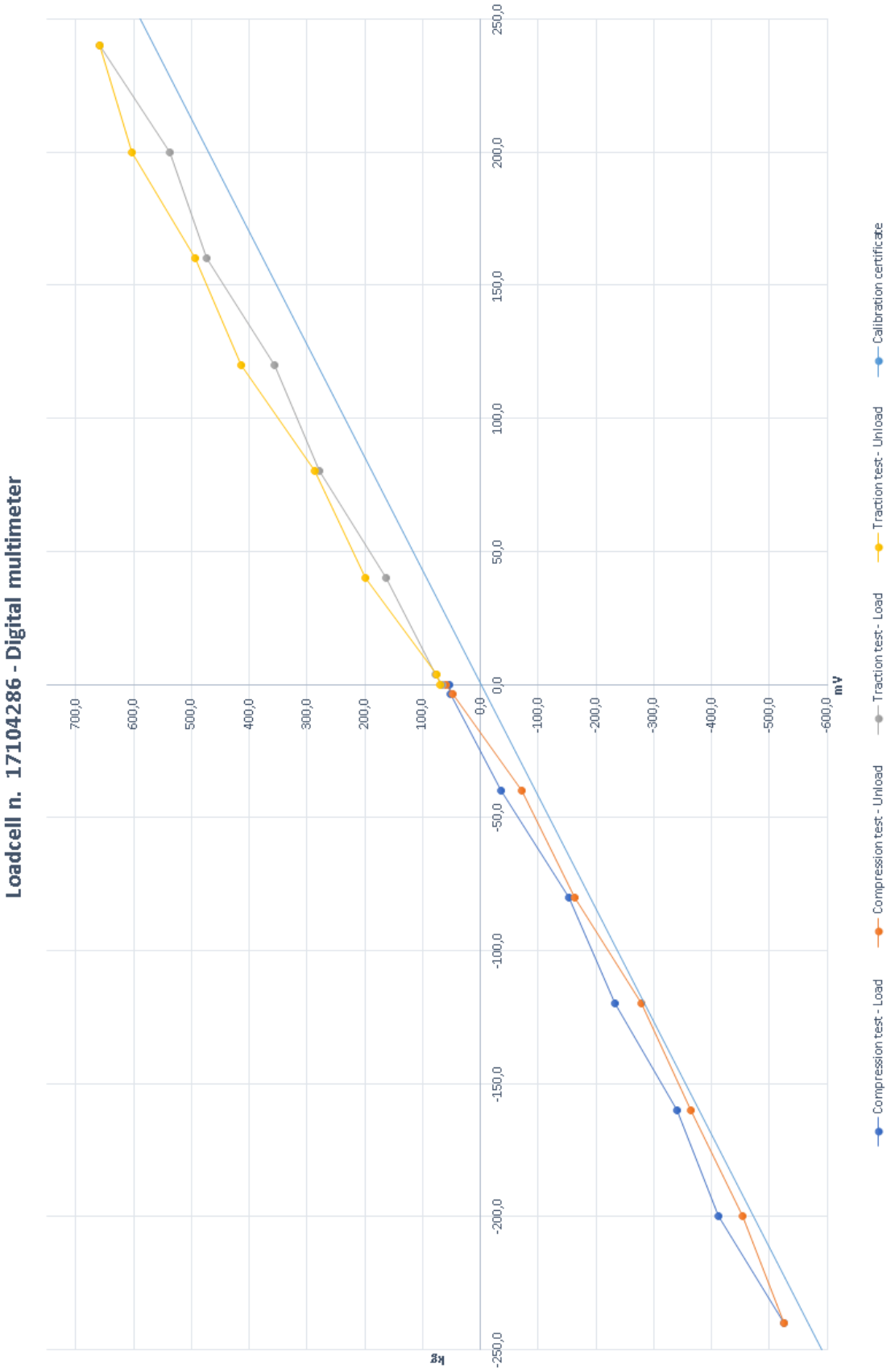

Figure 3.14: Tests output, load cell n. 17104286, data acquired with a digital multimeter.

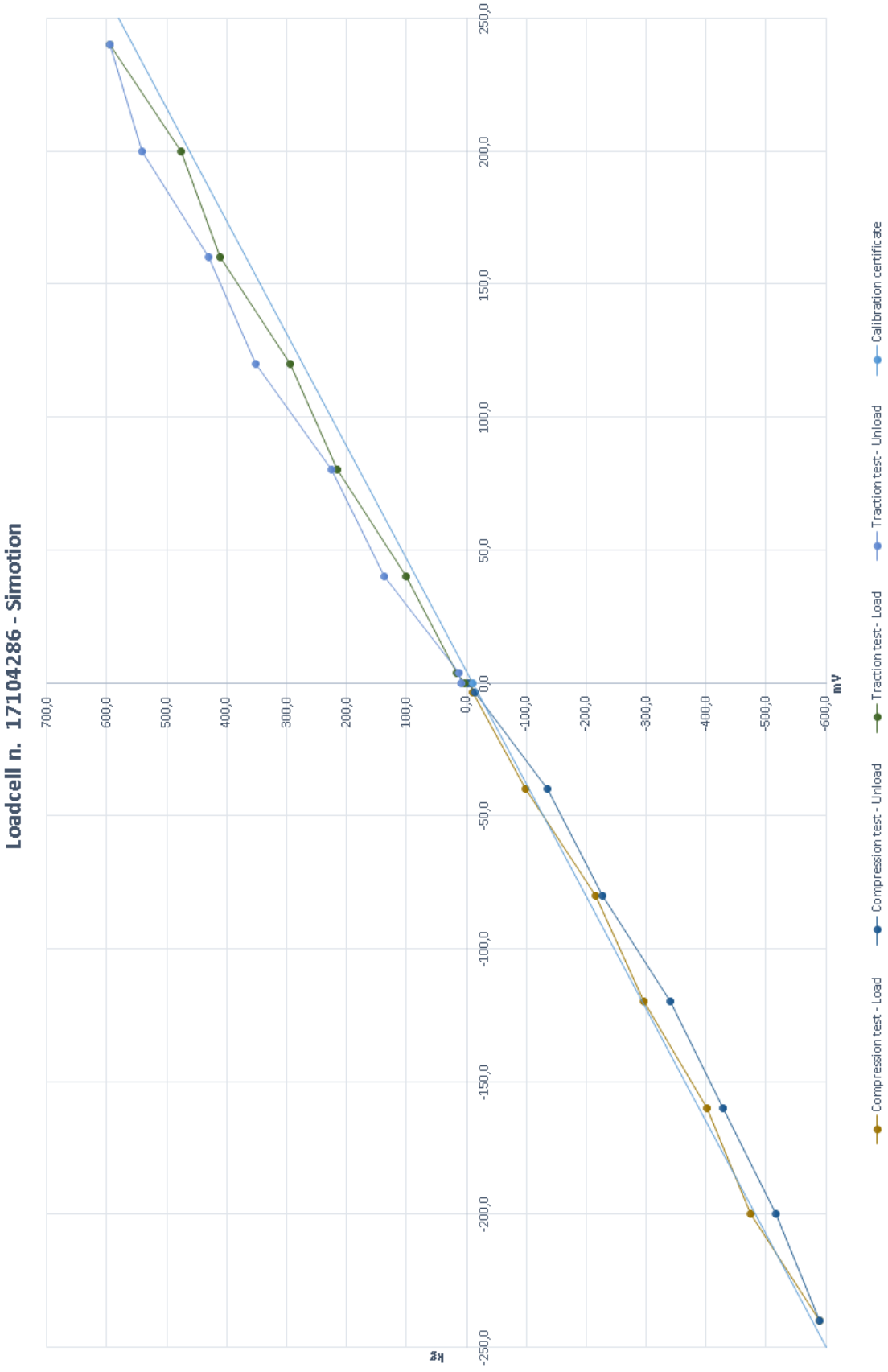

Figure 3.15: Tests output, load cell n. 17104286, data acquired with Simotion.

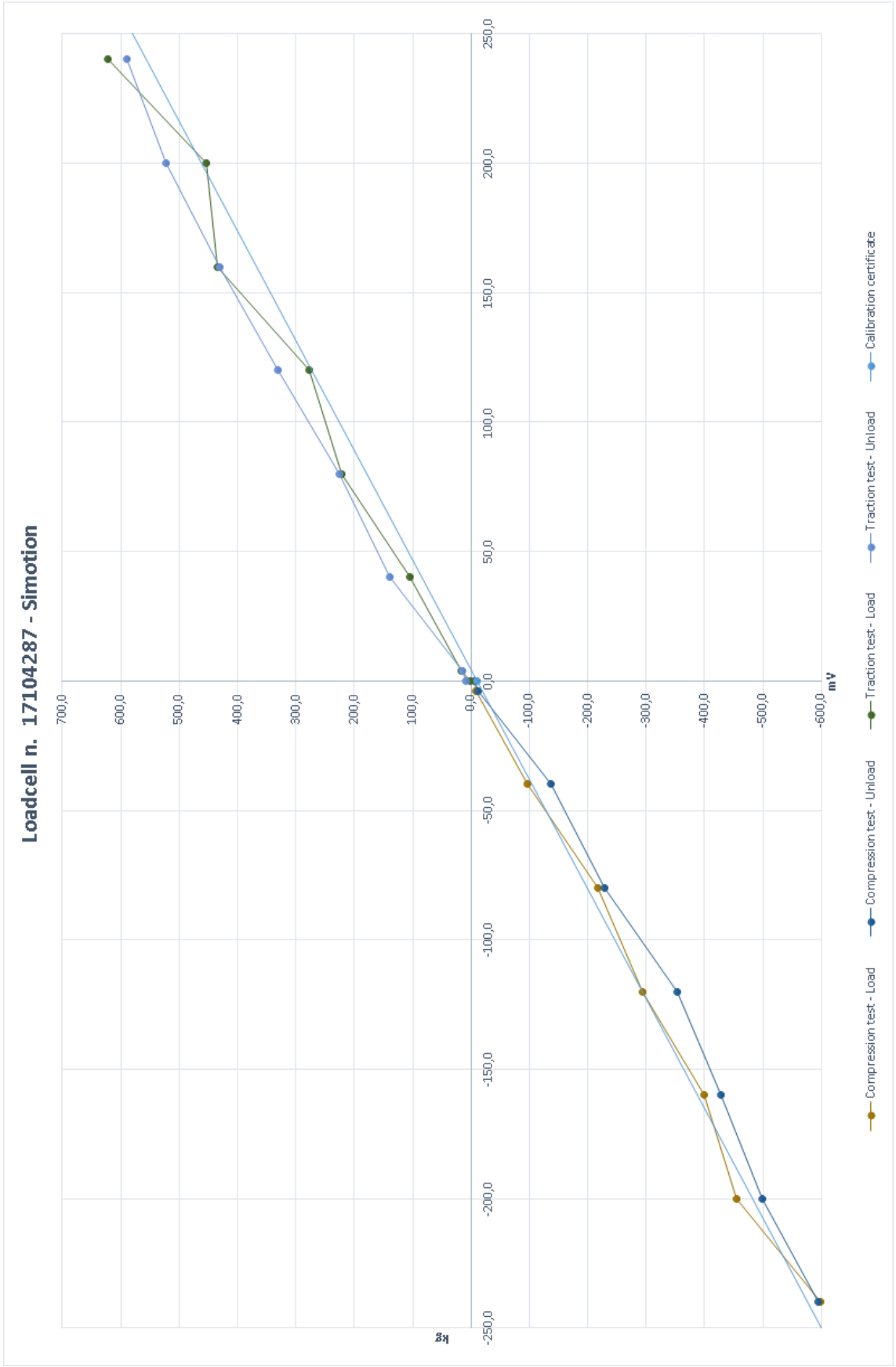

Figure 3.16: Tests output, load cell n. 17104287, data acquired with Simotion.

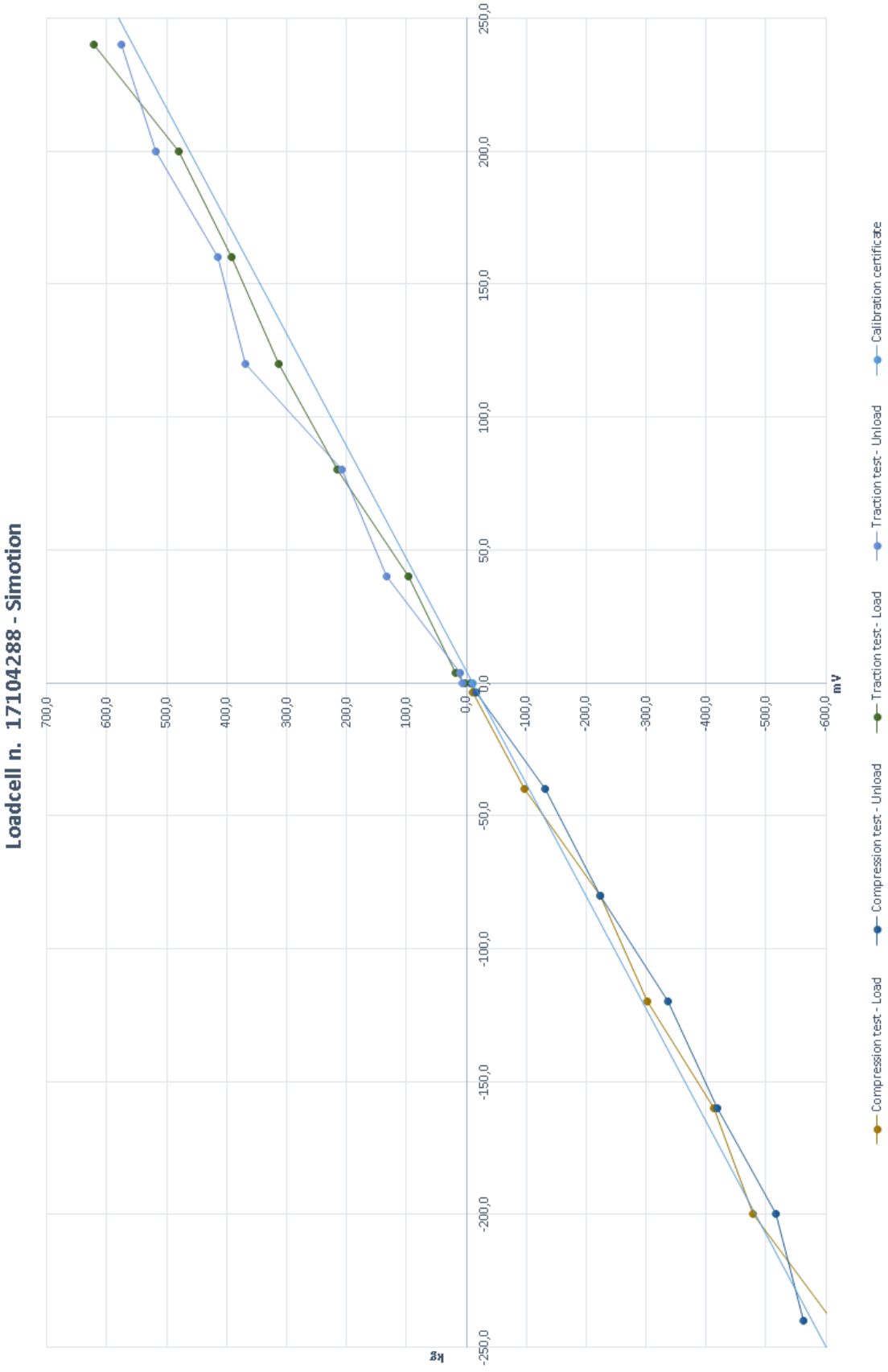

Figure 3.17: Tests output, load cell n. 17104288, data acquired with Simotion.

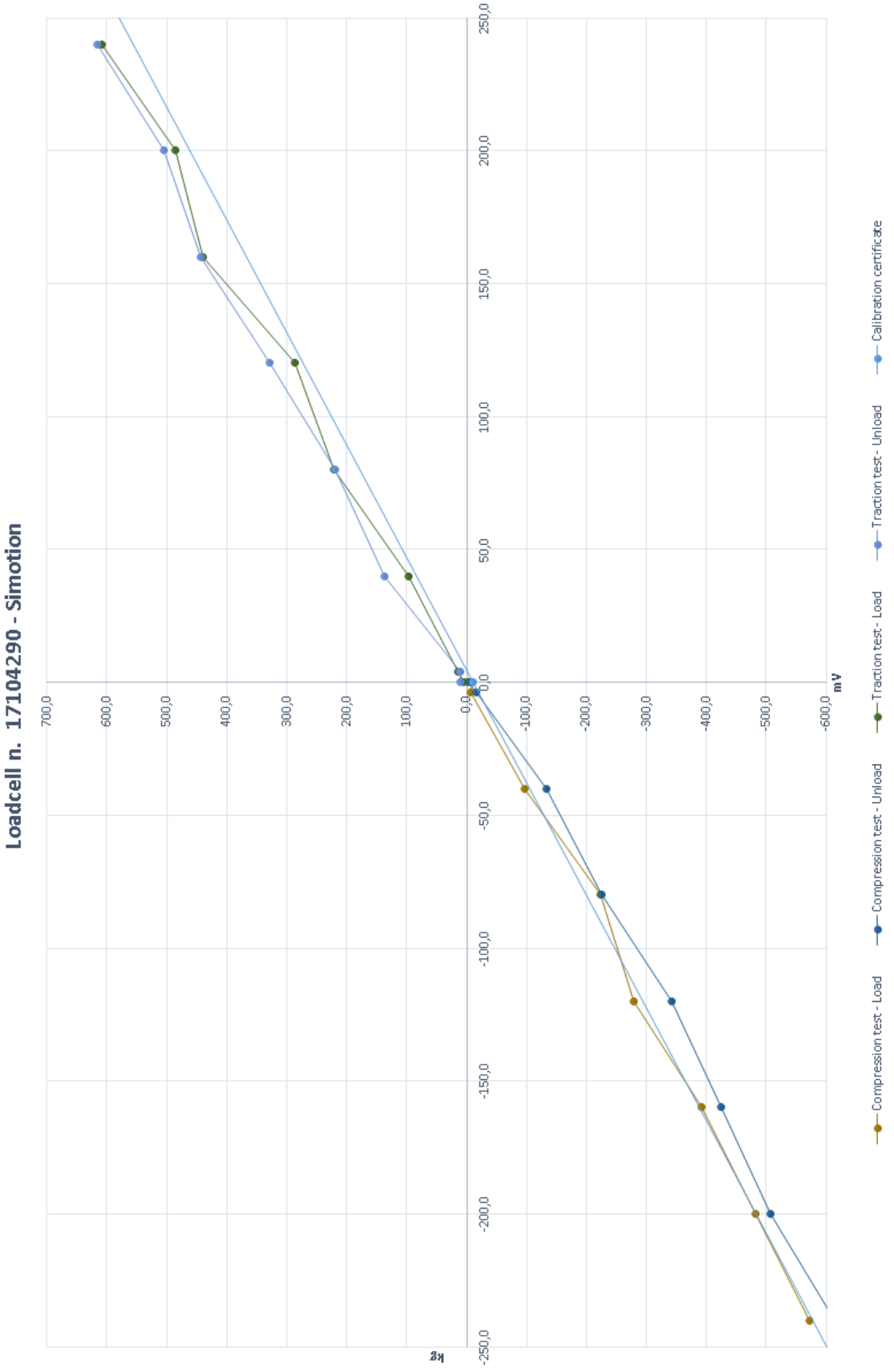

Figure 3.18: Tests output, load cell n. 17104290, data acquired with Simotion.

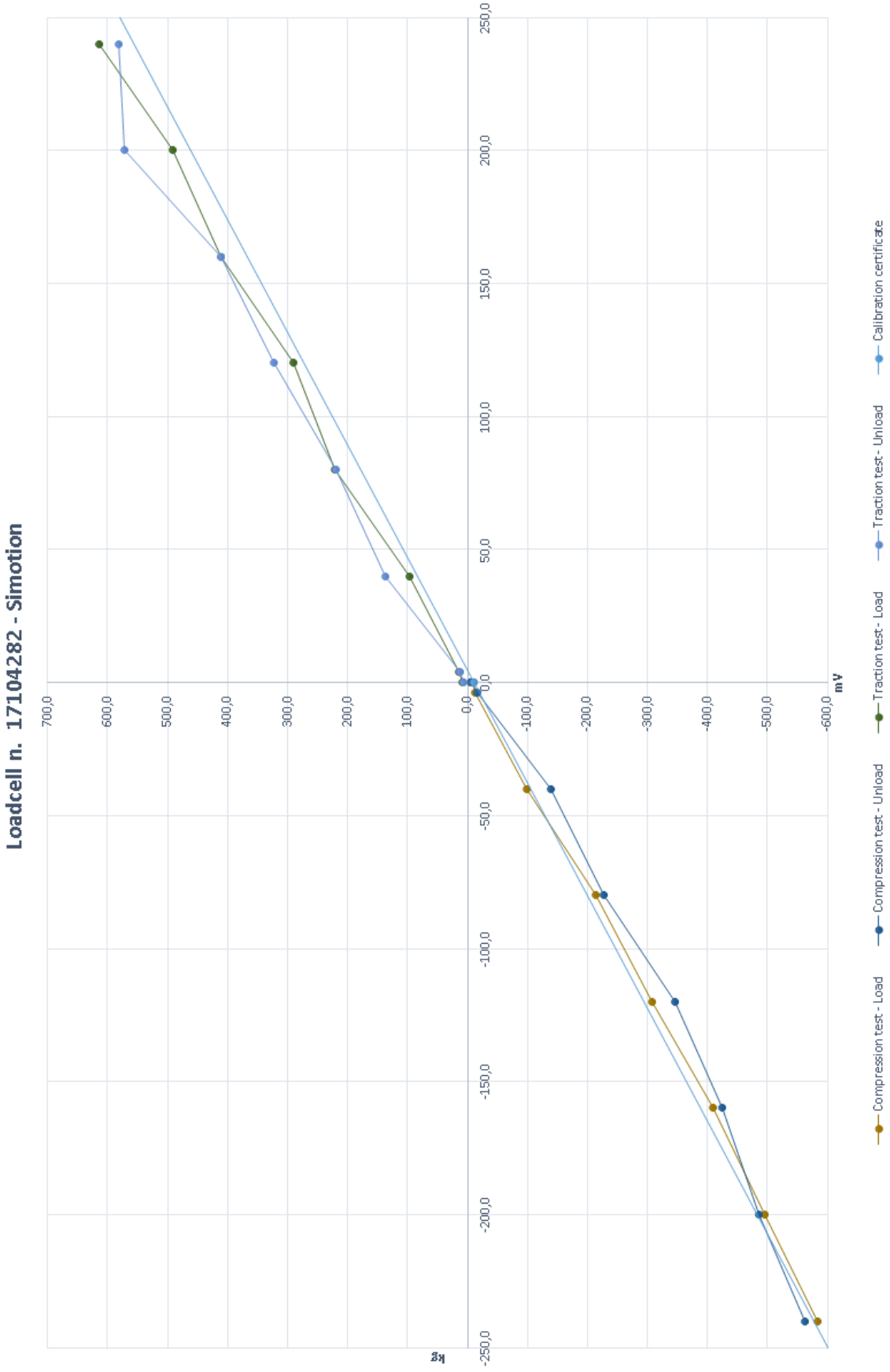

Figure 3.19: Tests output, load cell n. 17104282, data acquired with Simotion.

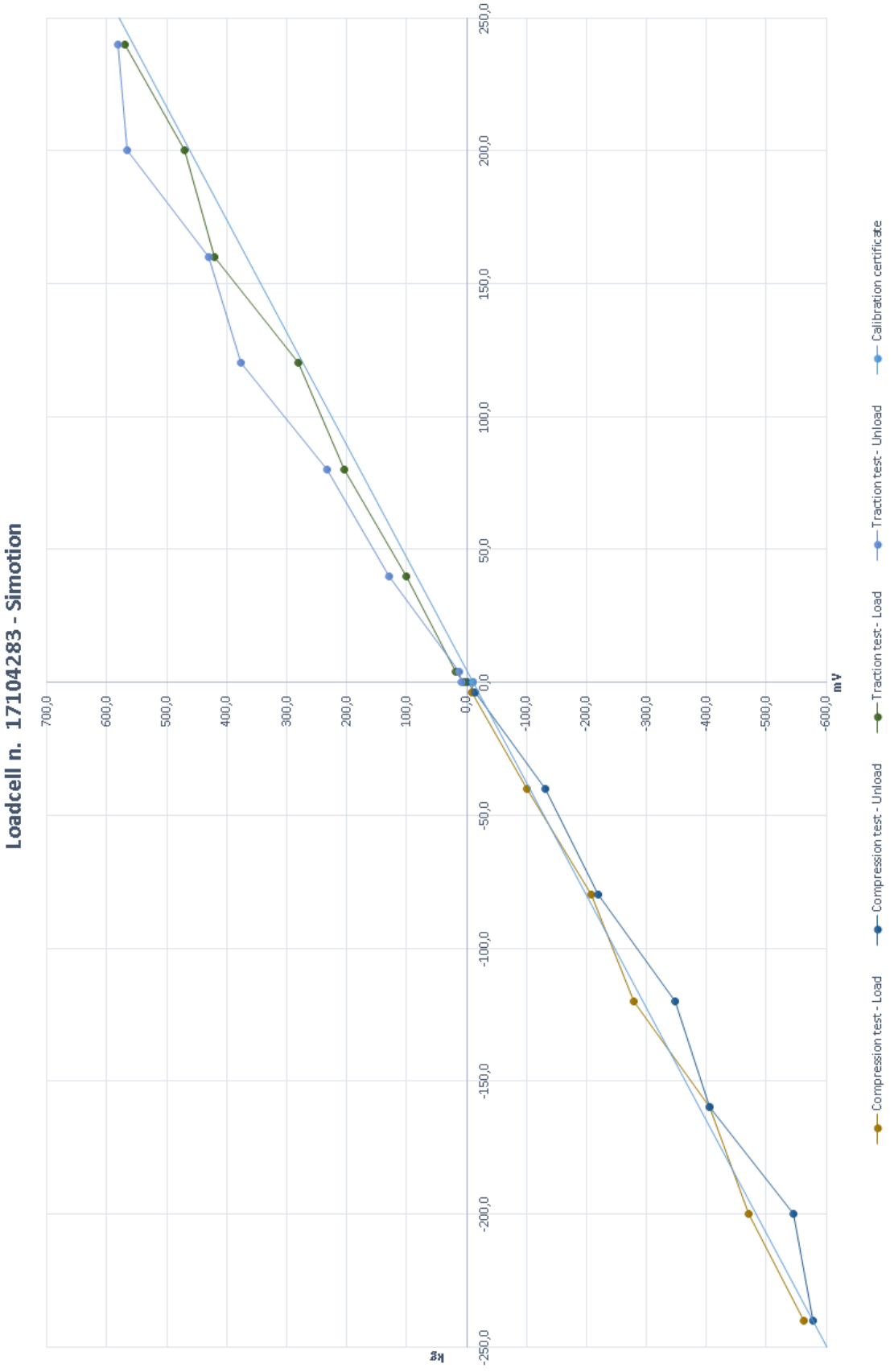

Figure 3.20: Tests output, load cell n. 17104283, data acquired with Simotion.

Chapter 4

Meteo station system

This chapter is about the integration on the prototype of Kitenergy s.r.l. of a Wind station able to detect wind direction and speed. The selection criteria among various types available on the market are discussed. The tests to correctly set up the weather station are described along with the electronics schematics. A brief discussion on the software written to collect data ends the chapter.

4.1 The problem

Correctly sensing and monitorizing the wind at least at ground level is crucial in order to develop a robust autopilot that can fly in any circumstances, reliable and stable. Data about wind intensity and direction at ground level are useful for this purpose but also ti have a better understanding about the intensity and direction of the wind at higher heights above ground level. The main objective is to produce energy by converting mechanical power into electric power via generators and a power kite. Since the kite needs to fly in a certain wind window, knowing the wind direction becomes a crucial asset. There are different flight phases, some in which the kite unrolls the cables producing energy and some in which the kite is pulled back close to the ground station and energy is consumed. Since the rolling or unrolling speed has to be around one third of the wind velocity, knowing the wind speed also becomes very important.

4.2 The Wind station

Considering the circumstances, a meteo station has been accurately selected among the various producers. The model adopted for the purpose is composed of a wind trasmitter: *Wind Transmitter "First Class" Advanced4.3351.10.000* and by a *Wind Direction Transmitter "First Class" 4.3151.00.400*, both developed and produced by *Thies Clima*, located in Germany. The FirstClass anemometers and wind direction transmitters are designed to sense the horizontal component of the wind velocity in the field of meteorology and environmental measuring technology. The possibility to evaluate the location and astimate the capacity and the characteristics of wind power systems is very important considering the application field and the nature of the prototype discussed in this paper. The weather station here discussed is perfectly suitable for the intended application and, moreover, for data acquisition in harsh or even extreme environments. It's important to remember that the anemometer and

the wind direction transmitter meet all requirements of IEC 61400-12-1 (2005-12) for an instrument of the accuracy class 0.5 and therefore also help raising the overall TRL level of the technology.

4.2.1 The Wind direction transmitter

The characteristics of the sensors, defined and optimized in its dynamic behaviour, are the following:

- High measurement accuracy and resolution.
- High damping with small distance constant.
- Low starting value.
- Low power consumption.
- Simple mounting.

The measuring value is available at the output as digital signals. The output signal can be therefore transmitted to display instruments, recording instruments, data loggers as well as systems designed for process control. Most of all, the digital output of this wind direction transmitter can be added to the output serial data telegram of the wind anemometer. The complete list of the characteristics is reported in Table 4.1 and the sensor is visible in Figure 4.1.

As reported by the constructor, the dynamic characteristics of the wind vane is achieved by the anodized aluminum lightweight construction. The co-action of the wind vane and the balance weight results in a high damping ratio with small delay distance. The axis of the wind vane runs on spherical ball bearings and carries a diametrically magnetized magnet at the inner end. The angle position of the axis is scanned contactless by a magnetic angle sensor (TMR Sensor, a Tunnel Magneto Resistance) through the position of the magnet field. As the sensor is operated in magnetic saturation, effects by external magnetic fields can almost be eliminated. The connected electronics calculates the angle position of the axis and provides the respective serial output signal. The outer parts of the instrument are made of corrosion-resistant anodized aluminum, and stainless steel. The sensitive parts inside the instrument are protected against humidity and dust through O-rings and highly effective labyrinth gaskets.

4.2.2 The anemometre transmitter

The characteristics of the sensors, defined and optimized in its dynamic behaviour, are the following:

- Works at high turbulence intensity.
- Minimal over-speeding.
- Low starting value.
- Low power consumption.

Wind direction transmitter	
Parameter	Value
Measuring range	0 ... 360°
Measuring Accuracy	±1°
Resolution	0.1°
Output telegram	<STX>XX.X XXX.X*HL<CR> <ETX> ex. 15.3(m/s) 347.1(°)
Electrical output	RS 485 1200 ... 57600 Baud 8 Bit, no parity, 1 stop bit ASCII
Starting threshold	< 0.5 m/s at 10° acc. to ASTMD 5096-96 < 0.2 m/s at 90° acc. to ASTMD 5096-96
Measuring time	10 ms
Operating speed	Up to 75 m/s
Survival speed	85 m/s up to 0.5°h
Wind velocity input	1082 Hz at 50 m/s
Delay distance	< 1.8 m acc. to ASTMD 5096-96
Damping ration	> 0.3 acc. to ASTMD 5096-96
Quality factor	K > 1 $K = \frac{4D\omega_0}{\rho u}$ D damping ratio ω_0 angular fr. of undamped oscillation ρ air density u wind speed
Connection	8-pole plug connection for shielded cable in the shaft
Operating voltage	3.3 ... 42V DC 1 mA at 3.3 V, 1.5 mA at 5V
Ambient temp.	-50 ... +80°C
Weight	0.7 kg
Protection	IP 55

Table 4.1: Wind direction transmitter specifications.

- Simple mounting.

The measuring value is available at the output as digital signal. The output signal can be transmitted to display instruments, recording instruments, data loggers as well as process control systems. Most of all, the digital output of this anemometer transmitter can be added to the output serial data telegram of the wind direction transmitter. The complete list of the characteristics is reported in Table 4.2 and the sensor is visible in Figure 4.2.

A low-inertia cup star with 3 cups, made in carbon-fibre-reinforced plastic, is set into rotation by the wind. The rotation is scanned opto-electronically, and is

Figure 4.1: The wind direction transmitter.

converted into a square wave signal. The frequency of this signal is proportional to the number of rotations. Depending on the supply voltage, the output signal ranges between maximal output voltage and ground of a potential zero (life-zero), lifted of 1.2 V. To efficiently supply all of the electronics, a minimal of 3.3 Vdc, up to 48 Vdc, is needed. The current consumption is very low. The outer parts of the instrument are of the same material as the wind direction transmitter, therefore it is dust and water proof. The instrument is mounted onto a mast tube while the electrical connection, with all the plugs, is located inside the shaft of the transmitter.

4.2.3 Wiring

The connection of the cable shield between sensor and the prototype has been done in order to avoid any case of over-voltages and equalizing current flows that might damage, or in the worst case even destroy, the electronic components. The cable used has a diameter of 7.6mm and a core cross-section of 0.5 mm^2 to the enclosed coupling socket per wire with 8 wires. In Figure 4.4 it's possible to see the configuration of the cable mounting while in Figure 4.3 the coupling socket is depicted: it is a Binder type, Serial 423, EMC with cable clamp. The supply voltage and the ground are given by the prototype, at 24 V DC.

In Figure 4.5 there is the connection diagram for the wind direction transmitter

Anemometertransmitter	
Parameter	Value
Measurement range	0.3 ... 75 m/s
Accuracy	1% of meas. value or <0.2 m/s
Output form	rectangle, edge steepness < 1μsec
Output frequency	1082 Hz at 50 m/s
Output amplitude	supply voltage, max. 15 V
Output resistance	130 Ωat 5 V
	230 Ωat 3.3 V
	Constatnt power limiting 25 mA
Linearity	Correlation factor r between frequency and wind speed
	$y = 0.0162 * f + 0.21$ typical
	$r > 0.999$ for 4 ... 20 m/s
Starting velocity	0.3 m/s
Resolution	0.05 m wind run
Distance constant	<3 m acc. to ASTM D 5096-96
	3 m acc. to ISO 17713-1
Turbulent flow	Deviation Δv turbulent compared with stationary horizontal flow
	-0.5% < Δ < +2%
	Frequency < 2 Hz
Classification	According to IEC 61400-12-1
	Class A classification index A 0.9
	Class B classification index B 3.0
	Class S classification index S 0.5
Wind load	100 N at 75 m/s
Operating voltage	3.3 ... 48V DC
Current consumption	150 μA max. at 3.3 ... 15 V
	200 μA max. at 15 ... 48 V
Connection	8 pole plug connection for shielded cable in the shaft
Ambient temp.	-50 ... +80 °C
Weight	0.5 kg
Protection	IP 55

Table 4.2: Anemometer specifications.

while in Table 4.3 the different pins are enumerated and explained in their functionalities. The 25W pins, numbered as 8 and 9, have not been used.

In Figure 4.6 there is the connection diagram for the anemometer while in Table 4.4 the different pins are enumerated and explained in their functionalities. The pins numbered as 7 and 8 have not been used, as for the wind direction transmitter. The pins numbered as 5 and 6 have not been used as reported on the datasheet of the instrument.

Figure 4.2: The wind direction transmitter.

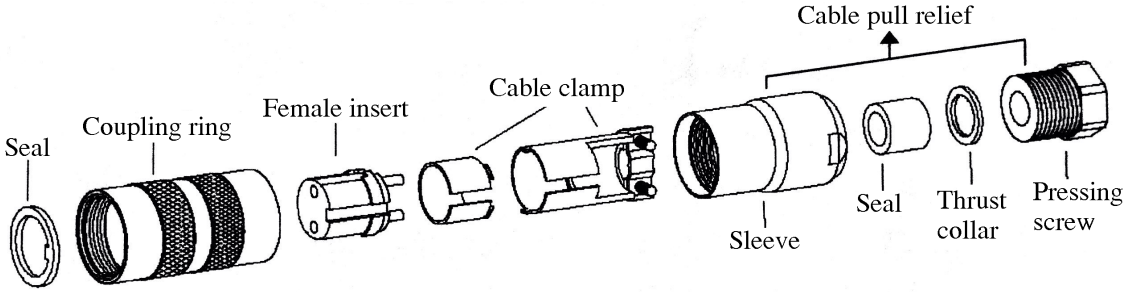

Figure 4.3: Cable coupling socket.

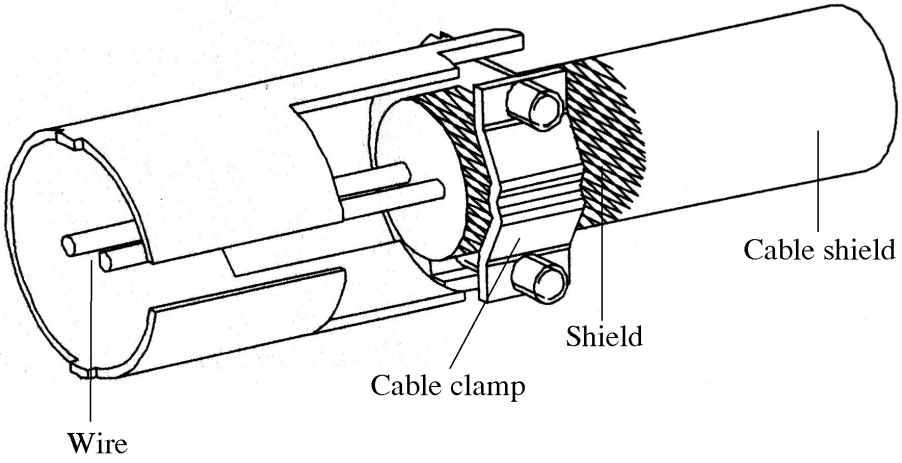

Figure 4.4: Cable connection.

Wind direction sensor pins		
Pin n.	Name	Function
1	Wave frequency	Input wind velocity
2	GND	Supply ground
3	+Vcc	Supply
4	Serial B	RS 485(B), synchron clock
5	Serial A	RS 485(A), synchron clock
6	DGND	Digital ground
7	not used	not used
8	not used	not used

Table 4.3: Wind direction sensor pins.

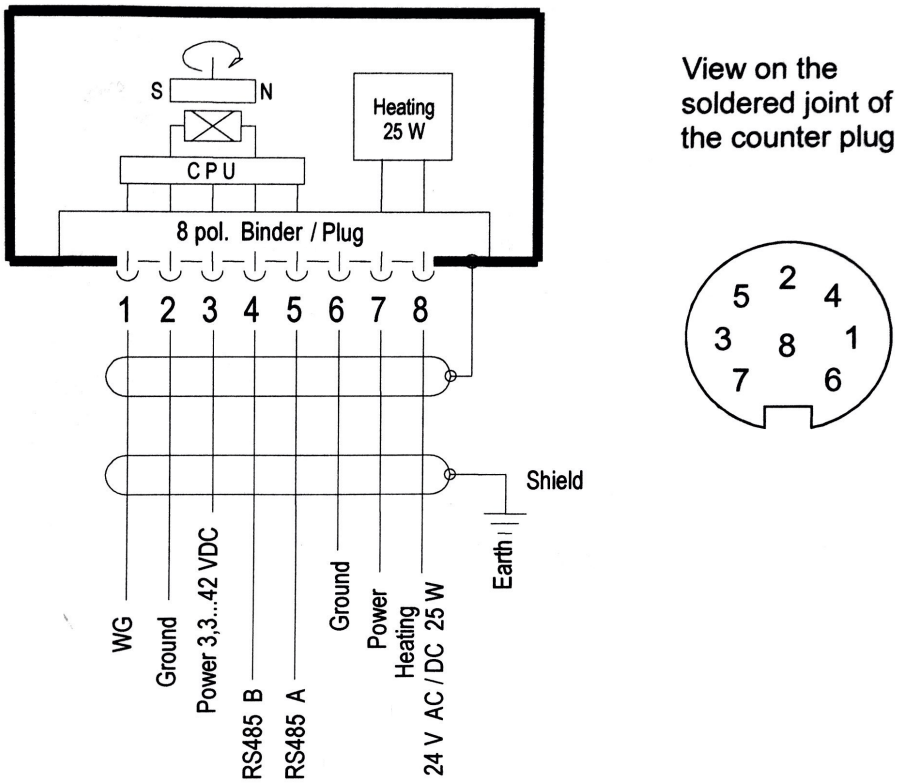

Figure 4.5: Wind direction transmitter connection diagram.

Anemometer sensor pins		
Pin n.	Name	Function
1	Signal frequency	Signal (rectangle)
2	GND	Supply ground
3	+Vcc	Supply
4	HGND	Ground at life-zero signal
5	not used	not used
6	not used	not used
7	not used	not used
8	not used	not used

Table 4.4: Anemometer sensor pins.

Data acquisition

The wind direction transmitter has been connected to a voltage supply and a RS485 interface, as in the connection diagram in Figure4.5. With the connection of the

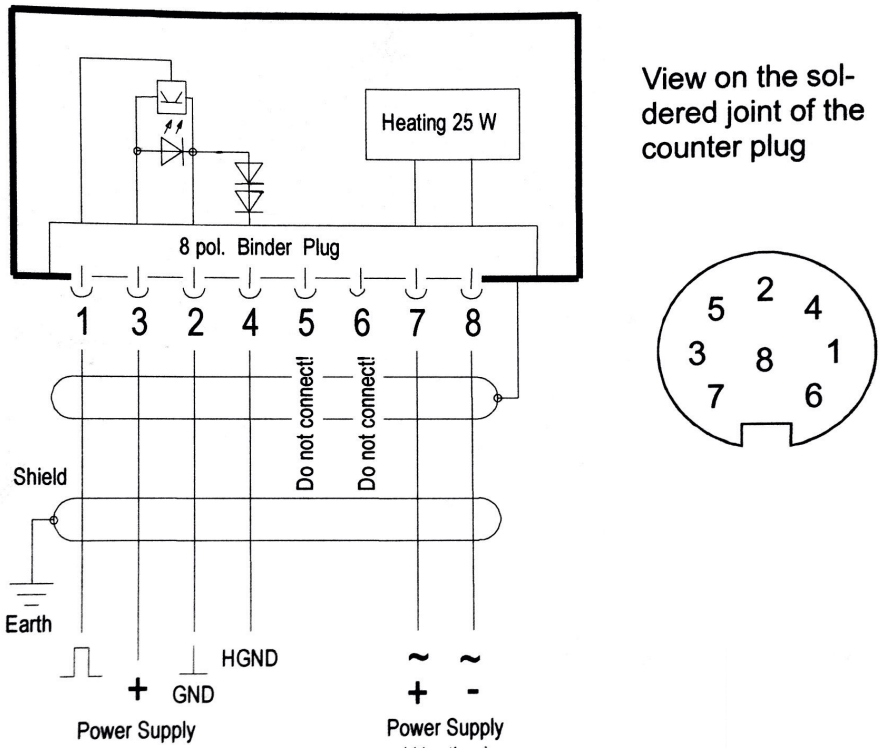

Figure 4.6: Anemometer connection diagram.

supply voltage and after a delay of 5sec, the output of serial data starts automatically with the following settings:

- Baud rate = 9600 baud.
- Data bits = 8 bit.
- Parity bit = no.
- Stop bit = 1.

For communication purposes the wind transmitter has a command interpreter through which it's possible to change the behaviour of the instrument. Some settings have been changed to better fit the communication requirements of the prototype presented in this paper, however such a detail it's out of the scope of this work. Still, some information are here discussed.

In Table 4.5 the meteo station's telegram is reported. On the left it's possible to see the character number while on the right column there is its description. The character n. 2, 3, 5, 7, 8, 9, 11 are logged into a microcontroller. Wind data are then appended to various other informations and sent to Simotion.

Testing

A test-bench has been set up in order to test the script that collects wind data and to test the various instruments. In Figure 4.7 it's possible to see the squared waveform of the anemometer on the oscilloscope: a squared waveform with a duty-cycle linearly proportional to rotational velocity of the cups. In Figure 4.8 there is a screen shot of the terminal window during a test: it's possible to see the serial telegram as it is described in Table 4.5.

Telegram construction	
Char n.	Description
1	STX (HEX 02)
2	10^1 wind velocity
3	10^0 wind velocity
4	Decimal point (HEX 2E)
5	10^{-1} wind velocity
6	Space (HEX 20)
7	10^2 wind direction
8	10^1 wind direction
9	10^0 wind direction
10	Decimal point (HEX 2E)
11	10^{-1} wind direction
12	'*' (HEX 2E)
13	H = high nibble check sum
14	L = low nibble check sum
15	CR (HEX 0D)
16	ETX (HEX03)

Table 4.5: Meteo station telegram.

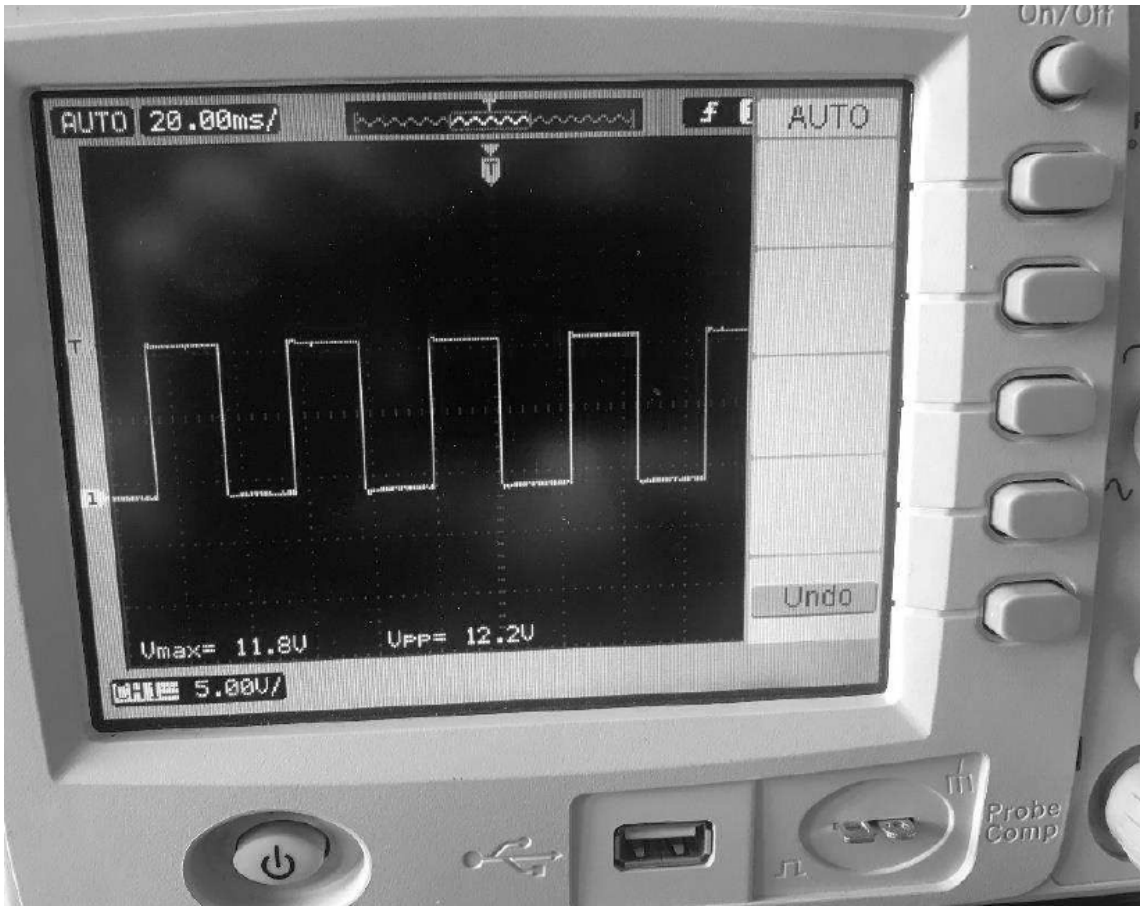

Figure 4.7: Squared waveform of the anemometer.

Sensor integration

The installation of the wind monitoring system on the KE-60 mkII prototype has been done by using a mast 8m long attached with screws on the side of the prototype.

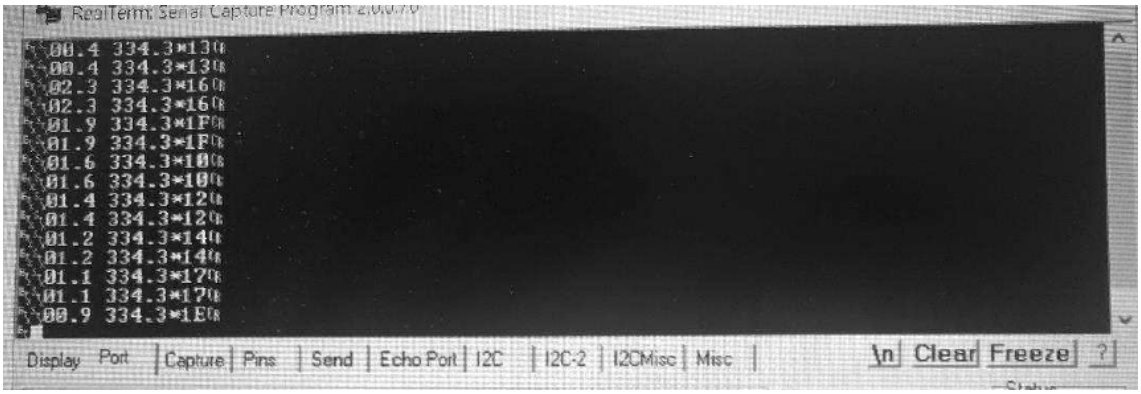

Figure 4.8: Wind data test readings.

The material is anodized aluminum. The cables nicely fit into the hole of the must ending in a IP 65 protected socket. In Figure 4.9 the prototype designed and built by Kitenergy s.r.l. is on the field for some test flights. The wind station described in this work it's perfectly visible on the side.

Figure 4.9: Wind station installed and working on the field.

Chapter 5

Conclusions and future developments

This chapter briefly makes an overview of the entire work, describing the circumstances that lead to this research; describing the current prototype designed and build by Kitenergy s.r.l.; refreshing the tension sensing system onboard the POD along with the Wind monitoring system; setting the conclusions.

5.1 Conclusions and future developments

In Figure 5.1 there is an overview of the data acquisition system described in this work. It has been embedded in the entire system of the Kitenergy s.r.l. prototype with the purpose of collecting data about the tension levels on the bridle system and monitoring wind speed and direction. The main goal is to collect data in order of being able, in the future, to design and develop an autonomous flight controller that can operate 24h in all the different flight phases.

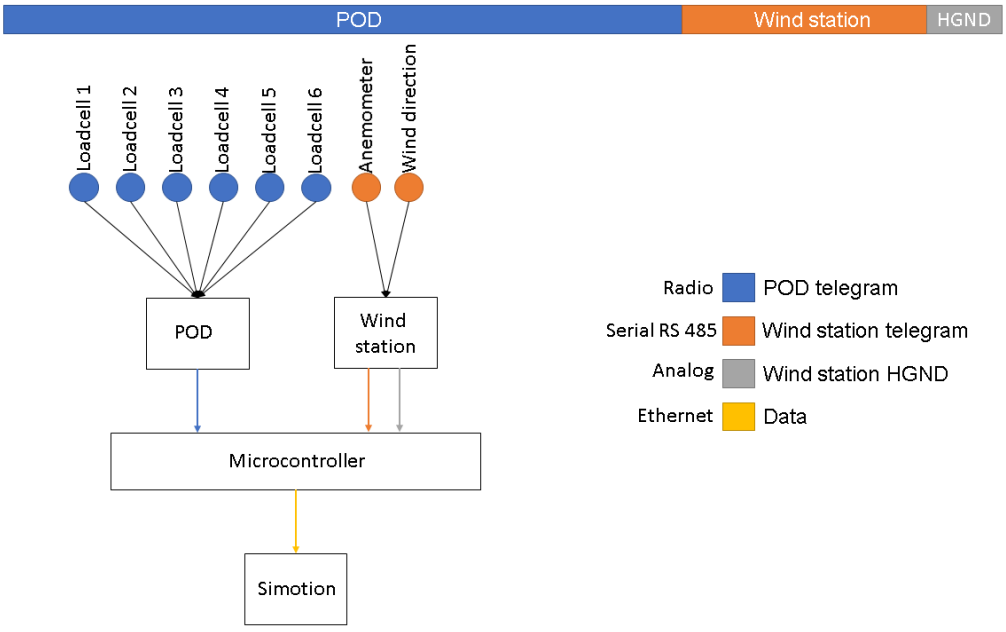

Figure 5.1: Overview of the communications described in this research.

Figure 5.2: The prototype during a test campaign with a beautiful sunset.

At the moment there is a variety of sensors onboard the POD that make the most of the final telegram sent to Simotion in terms of bytes. The loadcells are among them. The wind station telegram has been successfully appended to the POD telegram and a fault analysis has been done. The last byte is the HGND, which communicates if there is an absolute situation of no wind - in this case the anemometer is zero and the wind direction transmitter is static - or the wind station has been damaged and is not working anymore, being unable to detect wind. It's imperative, in case of remote controlling, for maintenance and reliability. Furthermore, the HGND is important to detect various other situations which discussion is out of the scope of this work. In the future new sensors may be added to collect new data that can help developing and consolidating the HAWE technology.

The HAWE technology still has to be fully understood by governments and institutions. However its potential is very well known among those that work in the filed of renewable energies and in the wind energy sector. Only through honest collaboration and cooperative and ethical work funds, research and development are possible and the HAWE technology will be finally hitting the market, providing 100% of renewable energy to remote and isolated areas that are in need; creating new jobs and new markets; pushing the boundaries of controls and automation to new levels and, finally, sparking the imaginations of dreamers around the world to find new ideas and fight for new ethical and environmentally clean solutions that can help everybody living a better life.

Bibliography

[1] M. L. Loyd. "Crosswind kite power". In: *Journal of Energy* (1980).

[2] G. M. Maneia. "Aerodynamic study of airfoils and wings for power kites applications". Master Thesis. Politecnico di Torino, 2007.

[3] L. Fagiano. "Control of Tethered Airfoils for High-Altitude Wind Energy Generation". Phd Dissertation. Politecnico di Torino, 2009.

[4] M. Furlan. "Modeling the Flight Dynamics of Tethered Wings for a Kite Energy Conversion System". Master Thesis. Politecnico di Torino, 2012.

[5] U. Ahrens, M. Diehl, and R. Schmehl. *Airborne Wind Energy*. Springer, 2013.

[6] M. Milanese, F. Taddei, and S. Milanese. "Design and Testing of a 60kW Yo-Yo Airborne Wind Energy Generator". In: *AirBorn* (2013).

[7] A. Cherubini et al. "Airborne Wind Energy Systems: A review of the technologies". In: *Elsevier* (2015).

[8] W. Ostachowicz et al. *Mare-Wint*. Springer, 2016.

[9] Albert Ludwing University of Freiburg and Delft University of Technology. *Airborne wind energy conference, Book of abstracts*. Albert Ludwing University of Freiburg, Delft University of Technology, 2017.

[10] G. Garibaldi. "Progetto di un impianto di produzione di energia elettrica per applicazioni eoliche di alta quota". Master Thesis. Politecnico di Torino, 2017.

[11] P. Rosafio. "From large-scale Aerodynamic Decelerator Systems to Airborne Wind Energy: Analogies, Similarities and Differences". Master Thesis. Politecnico di Torino, 2017.

[12] International Energy Agency (IEA). *Electricity information: Overview*. IEA Publications, 2018.

[13] International Energy Agency (IEA). *World Energy Outlook 2018*. IEA Publications, 2018.